PEATLAND CARBON STORAGE IN SOUTHERN PATAGONIA: FROM LONG-TERM LEGACIES TO SHORT-TERM DYNAMICS

A Thesis

by

MICHAEL SETH BUNSEN

Submitted to the Office of Graduate and Professional Studies of
Texas A&M University
in partial fulfillment of the requirements for the degree of

MASTER OF SCIENCE

Chair of Committee,	Julie Loisel
Committee Members,	David Cairns
	Brendan Roark
	John Giardino
Head of Department,	David Cairns

May 2020

Major Subject: Geography

ABSTRACT

Peatlands have been important terrestrial carbon reservoirs throughout the Holocene, yet whether these ecosystems will become stronger carbon sinks in the future remains debated. While surface peat layers have a greater apparent rate of carbon accumulation than deeper, millennial-aged peat, it is difficult to project how much more aerobic decomposition will take place before the younger surface cohorts join the older deeper ones, and thus whether ongoing environmental change and human activity are promoting or impeding carbon sequestration. Indeed, processes in the upper, periodically aerobic portion of a peatland (called the acrotelm) are particularly important because this is where peat formation occurs. Over decades to centuries, the young peat in the acrotelm gets progressively incorporated into the permanently anaerobic portion of the peatland (called the catotelm), where decay almost ceases. Studies have suggested that warming could lead to weakened carbon accumulation in peatlands due to enhanced aerobic decay in the acrotelm, which would lead to a slower transfer of peat into the catotelm, if at all. Conversely, other studies have suggested greater C accumulation in the acrotelm and thus, greater long-term carbon transfer into the catotelm under warming conditions because of greater plant productivity and faster peat accumulation. As a result of these contrasting processes, debate continues over the net effect of climate and land-use change on peat carbon stocks in the future. The acrotelm remains a challenging layer to study given its dynamic nature and the difficulty in dating it as well as in isolating the relative role of diagenesis and compaction vs. that of environmental change. Nevertheless, improving our predictions about the rate of present and future peatland development is important to forecast feedbacks on the global carbon cycle, and help inform land management decisions.

In my thesis, I analyzed a series of peat cores from southern Patagonia to calculate their long- vs. short-peat carbon accumulation rates. The acrotelm rates were then compared to the catotelm peat carbon legacies using an empirical modeling approach that allows calculating the future catotelm peat storage based on today's acrotelm characteristics, and thus predict if those recent rates of carbon accumulation will lead to greater or weaker long-term carbon storage in the future. I also compared the recent rates of carbon accumulation from Patagonia with those from global peatlands using a newly developed database that includes 186 sites. I find that, contrary to previous findings, Patagonian peatlands are not particularly effective at sequestering carbon on the short-term. That said, they are very effective long-term carbon reservoirs, in part perhaps due to their old age (often > 10,000 years). Lastly, the empirical models indicate that, depending on the local climate, some peatlands may become stronger carbon sinks in the future, while others may become weaker.

ACKNOWLEDGEMENTS

Firstly, I'd like to thank my M.S. Advisor Dr. Julie Loisel for her guidance and insight throughout my time as a graduate student at Texas A&M University (TAMU). Secondly, I'd like to thank my committee members Dr. David Cairns, Dr. Brendan Roark, and Dr. Rick Giardino for their assistance and support throughout the course of my research.

Many friends and family have provided me with guidance and support along the way, and have been immensely helpful in the process of obtaining my degree. I'd like to thank my wife Kaitlin Bunsen for putting up with the long hours and attention necessary to complete this process, as well as the emotional support I needed in order to succeed. I'd also like to thank my parents for supporting me in numerous ways, and always being willing to listen.

I'd like to thank Julia Hillin, Patrick Campbell, Natalie Jacobs, Kirsten Bevan Rydell, Eric Nutt, Dr. Andy Parsekian (University of Wyoming), and Dr. Clau Mansilla (University of Magallanes, Chile) for their help in the field and in laboratory analysis; Dr. Tom Guilderson for his direction and mentoring with radiocarbon dating at Lawrence Livermore National Lab's (LLNL) Center for Accelerated Mass Spectrometry (CAMS); Dr. Chris Maupin from TAMU's Stable Isotope Geosciences Facility (SIGF) for carbon isotope measurements; Dr. Angela Gallego-Sala (University of Exeter, UK) for assistance with the climate data calculations; and Dr. David Cairns (TAMU) for contributing his expertise to aid with statistical analysis.

CONTRIBUTORS AND FUNDING SOURCES

Contributors

This work was supervised by a thesis committee consisting of my advisor Dr. Loisel, and committee members Dr. Cairns and Dr. Roark of the Department of Geography, as well as Dr. Giardino of the Department of Geology & Geophysics.

Data collection in the field was a collective effort provided by Dr. Julie Loisel (Texas A&M University), Julia Hillin, Patrick Campbell, Natalie Jacobs, Kirsten Bevan Rydell, Eric Nutt, Dr. Andy Parsekian (University of Wyoming), and Dr. Clau Mansilla (University of Magallanes, Chile. Data or the peat core geochemistry in sections 2.3 and 3.1 were provided in part by Julia Hillin. Data for the carbon isotope analysis in sections 2.3 and 3.1 were provided by Dr. Tom Guilderson at Lawrence Livermore National Lab's (LLNL) Center for Accelerated Mass Spectrometry (CAMS) and Dr. Chris Maupin from TAMU's Stable Isotope Geosciences Facility (SIGF). Data for the climate analysis in sections 2.5 and 3.3 were provided by Dr. Angela Gallego-Sala (University of Exeter, UK).

All other data collection, synthesis, and analysis was conducted by the student with guidance from the advisor, Dr. Julie Loisel (Texas A&M University).

Funding Sources

Graduate study was supported by a teaching assistantship from Texas A&M University's Department of Geography.

Research and data collection were funded by the National Geographic Society (Exploration Grant to Loisel) and TAMU's College of Geosciences (High Impact Learning Experiences Program).

TABLE OF CONTENTS

LIST OF FIGURES

LIST OF TABLES

Page

1. INTRODUCTION

Under warmer global air temperature and shifting precipitation patterns, Earth's landscapes and ecosystems have been experiencing important changes in structure, function, and process (e.g., Rastetter et al., 1991, McGuire et al., 2009). For example, the high-latitude regions of the globe are experiencing some of the greatest and fastest climate warming, and regions that were previously too cold or dry are being colonized by new flora and fauna (Swann et al., 2010). Shrub expansion is another example of this change where the introduction of vegetation into previously uncovered areas is absorbing incoming shortwave radiation and subsequently reducing albedo (Myers-Smith et al., 2011). Arctic warming also promotes ice and snow losses both on land and at sea, reducing the region's albedo (Graversen et al., 2008), changing surface energy balance (Hansen et al., 2006), and rerouting water flow (Manabe and Stouffer, 1980). The response of peat-accumulating wetlands (peatlands) to a warming climate in these high latitudes may lead to greater rates of carbon (C) sequestration and expansion into previously uninhabitable landscapes (Gallego-Sala et al., 2018). Peatlands are particularly sensitive to climate change due to their dependence on precipitation and their constant exchanges of greenhouse gases with the atmosphere, which are temperature- and moisture-dependent (Yu et al., 2008; Cai et al., 2010). However, the future response of these landforms to shifting climatic regimes is uncertain, and given their large C stocks (500 ± 100 gigatons (Gt); Gorham, 1991; Yu et al., 2010; Yu, 2012), a better understanding of their sensitivity to climate is required. Several studies have suggested that with increasing temperatures or moisture deficits, there is potential for peatlands to shift from a net C sink to a net C source to the atmosphere (Ise et al., 2008; Dorrepaal et al., 2009). The C released from these ecosystems would take the form of carbon dioxide (CO_2) and methane

(CH_4), further feeding the positive feedback loop of climate warming (Updegraff et al., 2001; Dorrepaal et al., 2009; Turetsky et al., 2015). In addition to climate change, anthropogenic pressure on peatlands is widespread, including peat drainage for agriculture, forestry, grazing, and industrial-scale peat extraction, all of which remove the stored C from underground and release it back to the atmosphere (Frolking et al., 2011). As such, a recent study suggested that since 1960, peatlands globally have become consistent C sources to the atmosphere due to large losses of natural peatlands to land-use change and cumulative C emissions from drained sites (Leifeld et al., 2019). That said, under certain climate change scenarios, there could be a steady increase in the peatland C sink capacity over the next century: the warming that is experienced at high latitudes might effectively open up new regions for peatland expansion and increase the rate of C sequestration in some existing peatlands (Gallego-Sala et al., 2018). However, a full understanding of how long this effect will last and if it will fully offset the C losses experienced at warmer, low-latitude regions, is unknown. Whether peatlands will become stronger C sinks in the future thus remains unresolved and is a matter of speculations.

Short-term (decadal to centennial) changes in climatic conditions can result in long-term (centennial to millennial) effects on the capacity of peatlands to maintain a positive C balance (Friedlingstein et al., 2006). Net peat accumulation is a function of the positive balance between plant primary productivity (from photosynthesis) and peat decomposition (from heterotrophic respiration), and these processes are changing under shifting climate conditions. Plant growth is mainly dependent on growing season temperature and surface moisture, the latter being controlled by precipitation, snowmelt, and evaporation (Adkinson et al., 2011). Peat decay is primarily controlled by local hydrology (i.e, water table depth (WTD)), as well as nutrient levels (pH) and temperature (Clymo, 1965). We know that these weather and climatic controls vary

over space and time, and their effects on peatland structure and function (and associated C dynamics) have been documented in many regions. For example, a sustained drought, by lowering WTD, could lead to mineralization and emission of old C to the atmosphere in some regions (Keller et al., 2004). Likewise, peatland C release in the form of CH_4 and CO_2 has been shown to increase with increasing temperature (Keller and Bridgham, 2007). Conversely, drying conditions could lead to changes in plant community composition and subsequent increases in C sequestration (Loisel and Yu, 2013a). Despite a growing number of such empirical studies, it remains difficult to predict whether the recently accumulated peat at any given site will lead to an enhanced or weakened C sink capacity. Indeed, while numerous studies have analyzed millennial-scale C accumulation trends in peatlands, relatively few have focused on the shorter-term processes. This is because young peat (the acrotelm) that has undergone partial aerobic decomposition has a greater apparent rate of C accumulation than old peat, but it is difficult to project how much more decomposition will take place before it joins the permanently saturated portion of the peat profile (the catotelm). Making predictions for present and future peatland development rates on the basis of historical rates is puzzling (Belyea and Malmer, 2004) and difficult to accurately execute.

The overall goal of this study is to assess whether recent (past ~ 100 years) C accumulation rates in Patagonian peatlands are abnormally rapid, as suggested by recent studies (Loisel and Yu, 2013b; Lourençato et al., 2017). This idea comes from a few recent observations of very high C accumulation rates (e.g., 400cm of peat in 1000 years) in some southern Patagonian peatlands. The preliminary hypothesis is that, under maritime conditions, these peatlands benefit from year-round growing seasons, but their decay rate is reduced due to low temperatures (Loisel and Yu, 2013a). Using new peat-core data from peatlands across southern

Patagonia and modeling techniques, I compare recent peat accumulation rates at the site level to long-term (past 10,000 years) C accumulation histories of those same sites. I also compare southern Patagonian recent C stocks to global ones using a new data synthesis.

With increasing occurrences of positive shifts in the Antarctic Oscillation (AAO; Cai et al., 2003) and associated poleward contraction of the westerly wind belt, the southernmost extent of Patagonia has been, and will likely continue to, experiencing warmer and wetter climate (Weidemann et al., 2018). That being said, the effects of these hydroclimatic changes on the peatland C sink capacity remain largely unknown. I hypothesize that my sites, which are located in the southern portion of Patagonia, which is affected by the intensified AAO, have been experiencing a recent increase in productivity that should lead to higher rates of C sequestration over the long term. Overall, quantifying the sign and magnitude of current shifts in peatland C accumulation can help inform land management strategies and policy in the future.

2. METHODS

2.1 Study Region

Southernmost South America (SSA; 50-55°S) presents a climate system in which peatlands have developed under a unique set of conditions (Loisel and Yu, 2013b). As the only landmass at this latitude, SSA is strongly influenced by the southern westerly wind belt, a constant, prevailing wind flowing from West to East. The regional climate is largely controlled by these winds in conjunction with the topographical variation from the Andes Mountains (Garreaud, 2009). When the humid air flowing from the Pacific Ocean moves over SSA (south of 35° S), precipitation is at a maximum along the western portion of the Andean Mountains in Chile (Garreaud, 2009). As this air moves further East, it dries out and warms as it moves over Argentina and towards the Atlantic (Paruelo et al., 1998). This movement of humid air across the continent has created a climate regime in which peatlands have been able to proliferate within a narrow North-South band that follows the Eastern (lee) side of the Andes Mountains (**Figure 1**). It is also important to note that the westerly wind belt itself migrates and contracts following the seasons and over millennial timescales, as part of the global atmospheric circulation (Moreno et al., 2010). Today, the core of the westerlies lies around 55° S in austral summer and 33° S in austral winter (Lamy et al., 2010). Superimposed on these shifts is the AAO, which exhibits a strong control on regional climate in the southern hemisphere. In its positive mode, the AAO leads to warmer and wetter than average conditions over SSA (Gillet et al., 2006).

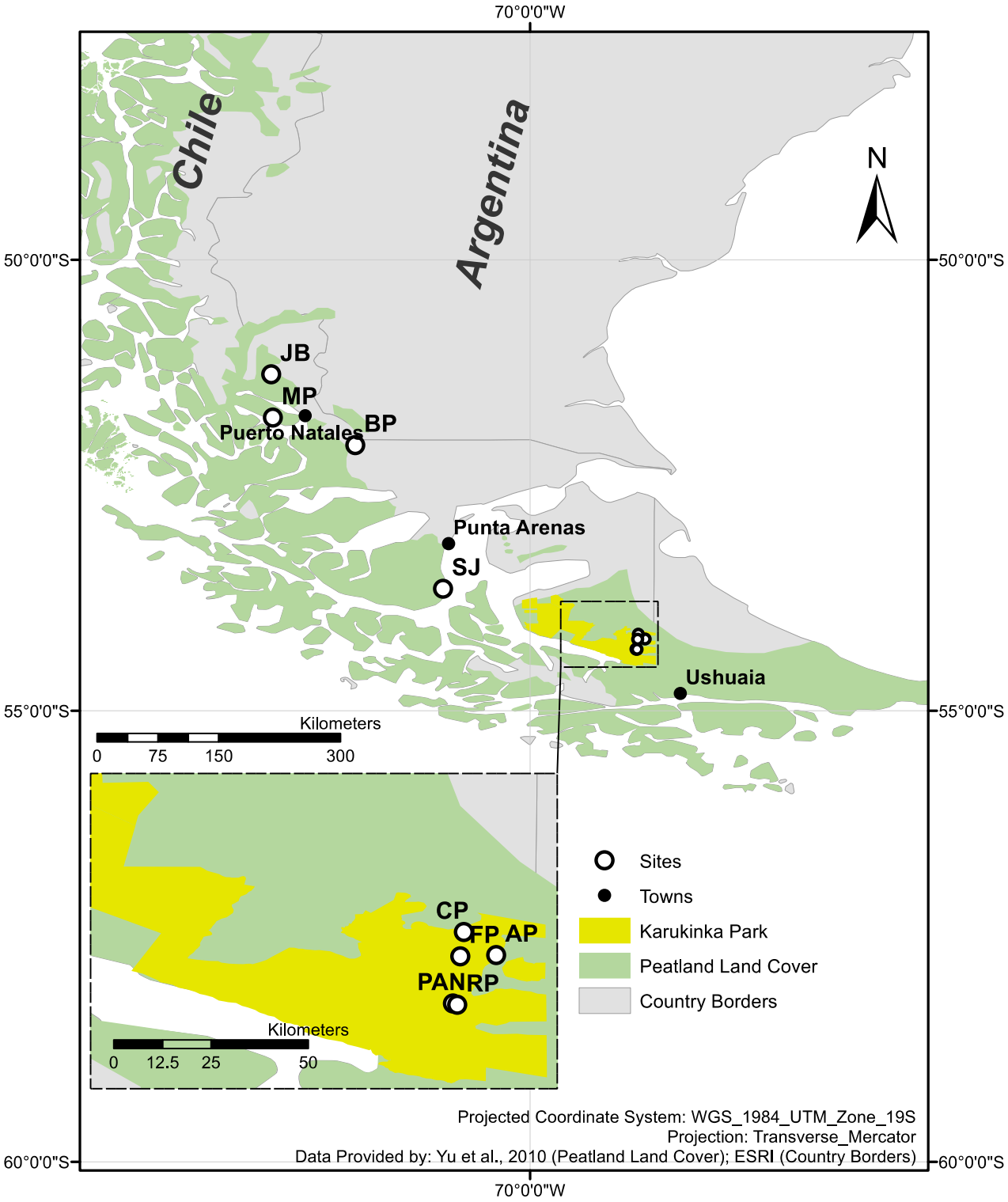

Figure 1. Study region and sites from southern Patagonia, South America. Shown are the peatland distribution (green area; Yu et al., 2010) and Karukinka Park boundaries (yellow area), as well as the main towns (closed circles) and peatland study sites (open circles; for site codes, see Table 1). The inset map shows the detailed coring site location within Karukinka Park in Tierra del Fuego.

Peatlands are abundant across the SSA region, and cover approximately 25% of the landmass (Loisel and Yu, 2013b). They are primarily distributed as a function of precipitation gradients: fens dominate the driest regions and are fed by groundwater, while cushion bogs are found in the wettest and windiest regions where annual precipitation is ~ 900-5000 mm (Auer, 1958; Moore, 1983; Pisano, 1983). Situated between these classifications are raised *Sphagnum magellanicum* peat bogs, which exist under cool and temperate climate, alongside the evergreen and deciduous forests, where the precipitation regime lies between ~ 400-900mm (Pisano, 1983; Grootjans, 2010). These peat bogs are exclusively rain-fed and tend to be restricted to low-gradient slopes and valley bottoms (Rabassa et al., 2006). These peat deposits often form over lacustrine sediments (Roig et al., 1996) or marine clays and silts (Bentley and McCulloch, 2005).

2.2 Study Sites and Field Sampling

Our team collected a total of nine cores from nine peat bogs across the Magallanes region of Chile, in SSA (**Figures 1 and 2, Table 1**). Four cores were extracted in mainland Chile, from sites located along the lee side of the Andes Mountains (north-south gradient spanning two degrees of latitude). The southernmost site (San Juan, 53.65° S) is located south of Punta Arenas, where the mean annual air temperature (MAAT) is 6.4° C and mean annual precipitation (MAP) is 442 mm/year (climate-data.org). The northernmost site (Jen Bog, 51.27° S) is found north of Puerto Natales, where MAAT is 6.7° C and MAP is 389 mm/yr (climate-data.org). The remaining five sites are located on Isla Grande in Tierra del Fuego, farther to the southeast (**Figures 1 and 2, Table 1**). The cores were collected near the eastern edge of the Karukinka Conservancy Park, inside the park limits. The climate in Tierra del Fuego is influenced by its proximity to the Atlantic Ocean, the Magellan Strait, and the Beagle Channel, and is characterized by a MAP range from 300mm/yr to 600mm/yr, and a cooler MAAT of 5° C

(Rabassa et al., 2006). Together, the westernmost site on the mainland (Jen Bog, 72.87° W) and the easternmost site at Karukinka (Ariel Peatland, 68.72° W) allow us to analyze cores spanning an east-west gradient of approximately 4 degrees longitude.

Table 1. Site information for the new peat cores collected in southern Patagonia, South America. Location, site code (for reference) and maximum depth are reported for each core.

Site Name	*Site Code*	*Site Location*	*Latitude*	*Longitude*	*Depth (cm)*
Beef-Penguin Peatland	BP	Magallanes	-52.057	-71.935	770
PANs Peatland	PAN	Tierra del Fuego	-54.319	-68.82	503
Mercedes Peatland	MP	Magallanes	-51.752	-72.849	434
Jen Bog Peatland	JB	Magallanes	-51.273	-72.866	590
San Juan Peatland	SJ	Magallanes	-53.649	-70.961	125
El Cura Peatland	CP	Tierra del Fuego	-54.154	-68.795	249
Flarks Peatland	FP	Tierra del Fuego	-54.21	-68.803	360
Rasmussen Peatland	RP	Tierra del Fuego	-54.322	-68.81	291
Ariel Peatland	AP	Tierra del Fuego	-54.207	-68.72	242

Every studied peatland was a peat bog dominated by a continuous carpet of *Sphagnum magellanicum* (**Figure 2**). Every site was characterized by microtopographic gradients of raised, dry hummocks interspersed with low, wetter, and sometimes submerged, hollows. The microrelief (hummocks and hollows) of this landscape is characteristic of ombrotrophic bog complexes across the region of SSA and Tierra del Fuego (Rydin and Jeglum, 2006). Shrubs *Empetrum rubrum* and *Astelia pumilia* were commonly identified across the sampled gradients, along with a few sedge and grass species including *Marsippospermum grandiflorum*, *Tetroncium magellanicum*, *Alopecurus magellanicus*, *Carex magellanica*, and *Carex curta*. Towards the northwest, the cypress tree *Pilgerodendron uviferum* was observed at a couple of sites (Mercedes Peatland and Jen Bog); this cold-resistant hygrophilous conifer is typically found

in hyper-humid habitats of Patagonia. Towards the south and east, cypress trees quickly vanish and are replaced by beech species *Nothofagus betuloides* and *N. antarctica*.

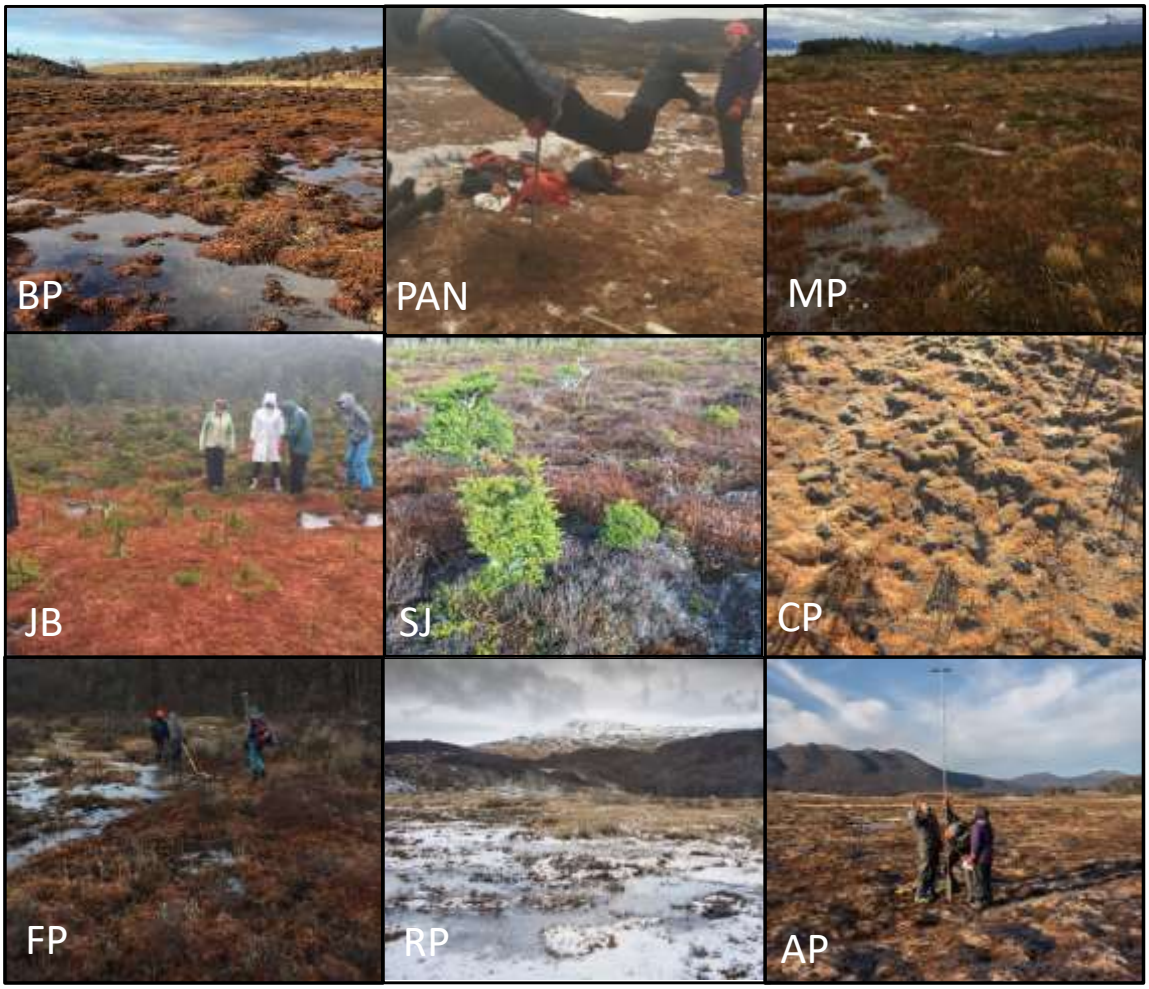

Figure 2. Photographs of all nine new peat bog study sites from southern Patagonia. Each site is dominated by a *Sphagnum magellanicum* carpet. Photo credits: Patrick Campbell, Michael Bunsen, and Julie Loisel.

All nine cores were collected in the austral fall (May and June) of 2018. The peat cores were extracted using a Russian-type coring device in 50cm increments and placed in half-cylinder PVC pipes to limit compaction during transportation. When possible, the surface peat

sections were recovered using a serrated knife. While these short monoliths (10 to 40cm in length) minimize surface compaction, they could not be retrieved when the peat surface was frozen. In these instances, the Russian auger was used to sample the entire peat profile. Peat cores were individually wrapped in plastic and foil to protect samples from contamination and water loss. Extensive notes detailing the main stratigraphic changes downcore in terms of peat types (moss, herbaceous, ligneous, etc.) and soil properties (texture, particle size, color, etc.) were taken in the field. The cores were then shipped to the Paleoecology Lab at Texas A&M University (TAMU) for further analysis.

2.3 Laboratory Analysis and Peat-Core Chronology

A series of standard geochemical analyses were performed along all nine cores. First, peat cores were cut into 2-cm slices that were then stored in plastic bags until further analysis. Loss-on-ignition (LOI) was conducted on every sample from each core. I used $2cm^3$ aliquots that were dried overnight in an oven at 105° C, weighed, then sequentially burnt at 550° C in a furnace for 4 hours, and weighed again. While samples lose their water during the first step, allowing us to determine peat dry bulk density (BD), CO_2 from organic matter is combusted during the second step, allowing us to determine organic matter content (OMC) (Dean, 1974). Peat cumulative mass (CM) was calculated along each core, from the bottom to the top, by multiplying OM content from each slice by its thickness and incrementally summing all values.

Peat-core chronologies were derived from radiocarbon (^{14}C) ages (**Table 2**). A total of 24 samples that typically consisted of hand-picked plant macrofossils were cleaned with deionized water, then dried and stored in foil. When peat samples were too decomposed for macrofossil identification and cleaning, dates were obtained on root-free bulk peat samples (63-125 µm). Samples were then graphitized (Vogel et al., 1987) and dated using accelerator mass

spectrometry (AMS) at Lawrence Livermore National Laboratory. Age-depth (A/D) models were developed using the program Bacon (version 2.3.5; Blaauw and Christen, 2011). Bacon constructs an A/D model by reading a file containing depth, ^{14}C ages with their associated error, and a calibration curve to construct accumulation rates throughout any given core. Bacon was preferred to constrain the peat accumulation histories because it doesn't develop A/D models linearly, where accumulation would be assumed to be constant between dated depths. Instead, Bacon divides the core into numerous vertical sections and runs millions of Markov Chain Monte Carlo (MCMC) iterations to determine the sedimentation rate along the profile (Blaauw and Christen, 2011). It uses the probability density function of each ^{14}C age and combines it with the relative location of each dated depth to produce the most probable age for each peat layer (i.e., a Bayesian approach). I used the default prior information settings for memory (shape = 4; mean = 0.7), and accumulation rate (shape = 1.5; mean = 20). In Bacon, ages are directly calibrated using a prescribed calibration curve. Given the location of my samples, I selected the SHCal13 calibration curve (Hogg et al., 2013; Reimer et al., 2013). I then used the Southern Hemisphere Zone 1-2 (SHZ 1-2) calibration curve (Hua and Barbetti, 2004) to determine the calendar age of samples younger than the nuclear weapons testing (called "post-bomb" samples). For the latter, CALIBomb (Reimer et al., 2004) was used to determine the age of each sample using the fraction modern ($F^{14}C$) notation; those $F^{14}C$ were then transferred to Bacon to develop the final chronologies. Dates are reported in calibrated years (cal.) before present (BP), where present is 1950 AD.

Table 2. Radiocarbon (^{14}C) dates for the new peat cores from southern Patagonia, South America. The analysis was conducted at Lawrence Livermore National Laboratory's Center for Accelerator Mass Spectrometry (CAMS). The fraction modern ($F^{14}C$) refers to 'post-bomb' samples. Each calibrated age range represents the 95% confidence interval (or 2 sigma range) for any given date; it was obtained using the SHCal13 calibration curve (Reimer et al., 2013). Each median calibrated date is the midpoint of the calibrated range. Median ages were calculated using Calib 7.10 software, except post-bomb dates marked with an asterisk (*), which were calibrated using CALIBomb. An assumed $\delta^{13}C$ value of -25 ‰ was used to calibrate the ^{14}C ages.

Core	*Depth (cm)*	*Dated Material*	*^{14}C Age (BP)*	*Fraction Modern (^{14}C)*	*Probability Range (2s cal. BP)*	*Median Probability Age ± 2s (cal. BP)*	*Bacon Median Age (cal. BP)*	*Lab ID (CAMS)*
BP	6-8	brown moss stems	> Modern	1.4766	(-14)-(-24)	-21 ± -5	-37	180898
	16-18	S. magellanicum stems	95 ± 30		252-(-6)	88 ± -129	121	180908
	26-28	S. magellanicum stems	330 ± 30		296-451	387 ± 77.5	344	180893
	36-38	S. magellanicum stems	520 ± 30		496-543	518 ± 23.5	519	180894
	298-300	root-free bulk peat (63-125µm)	6695 ± 30		7463-7586	7532 ± 61.5	7504	180903
	496-498	root-free bulk peat (63-125µm)	8605 ± 35		9477-9594	9533 ± 58.5	10070	180900
	768-770	root-free bulk peat (63-125µm)	13065 40		15339-15789	15594 ± 225	15547	180922
MP	14-16	S. magellanicum stems	> Modern	1.3963	(-14)-(-26)	-24 ± -6	-10	180907
	24-26	S. magellanicum stems	Modern	0.9934	248-(-7)	78 ± -127.5	111	180897
	34-36	S. magellanicum stems	Modern	0.9946	240-(-7)	56 ± -123.5	237	180895
	150-152	root-free bulk peat (63-125µm)	5630 ± 30		6300-6437	6362 ± 68.5	6356	180886
	320-322	root-free bulk peat (63-125µm)	9540 ± 35		10600-11072	10766 ± 236	10853	180888
	408-410	root-free bulk peat (63-125µm)	11895 ± 35		13567-13759	13664 ± 96	13682	180890
PAN	66-68	root-free bulk peat (63-125µm)	2995 ± 30		2990-3215	3111 ± 112.5	3095	180905
	168-170	root-free bulk peat (63-125µm)	5710 ± 30		6323-6549	6448 ± 113	6429	180902
	258-260	root-free bulk peat (63-125µm)	7045 ± 30		7742-7934	7843 ± 96	7865	180906
	378-380	root-free bulk peat (63-125µm)	8960 ± 35		9910-10191	10041 ± 140.5	9915	180901
	501-503	root-free bulk peat (63-125µm)	9540 ± 40		10590-11074	10772 ± 242	11158	180904
JB	568-570	root-free bulk peat (63-125µm)	5050 ± 30		5651-5892	5740 ± 120.5	5741	180891
SJ	12-14	S. magellanicum stems	> Modern	1.2425	(-13)-(-35)	-30 ± -11	36	180896
	22-25	S. magellanicum stems	Modern	0.9944	240-(-7)	59 ± 123.5	126	180899
	33-35	S. magellanicum stems	115 ± 30		253-(-6)	92 ± -129.5	236	180887
	43-45	S. magellanicum stems	190 ± 30		0-285	178 ± 142.5	382	180892
CP2	374-376	root-free bulk peat (63-125µm)	9305 ± 35		10290-10564	10442 ± 137	10411	180889

In the field and the lab, many layers of volcanic ash (tephra) were detected by visual examination of the peat cores and from LOI results, respectively. In the field, preliminary identification of the ash provenance was performed on the basis of texture and color, in collaboration with Dr. Claudia Mansilla (University of Magallanes, Chile). In the lab, samples with anomalously high bulk density and low organic matter content were observed under the microscope to confirm the presence of glass shards. As the regional tephrochronology is

relatively well known (Stern, 2008), the relative position of each tephra layer along our peat profiles was cross-correlated with that from other regional studies (Kilian et al., 2003; 2006). These dated tephra layers were used in conjunction with our A/D models in order to confirm our identifications. The tephra layers that could be visually identified within the stratigraphy of each core were included in the A/D models by excluding the incremental depth of the event. This increases the age-constraining for our models by accounting for the instantaneous vertical accumulation of volcanic ash as a single event as opposed to a gradual accumulation as that of peat growth.

By combining ^{14}C ages, identified tephra layers, and CM values, I produced peat accumulation histories for each of the nine cores. Long-term rates of C accumulation (LORCA) and recent rates of C accumulation (RERCA) were calculated for each peat slice by assuming a C content of 50% (Turunen et al., 2002; Loisel et al., 2014). Along our peat cores, the acrotelm/catotelm boundary was defined using the instantaneous rate of change (1^{st} derivative) of the A/D model, which corresponds to the interval showing the greatest change in rates between two adjacent samples. Water content values were used to confirm the position of the acrotelm/catotelm boundary, which was accompanied by a decrease in WC. As a reminder, the acrotelm is the top section of the peat profile, where intensive aerobic decay takes place. The catotelm is the thick and saturated peat section below the acrotelm where very slow anaerobic decay takes place over millennial timescales (Blodau, 2002). Over decades to centuries, the young peat in the acrotelm gets progressively incorporated into the catotelm, where decay almost ceases (Rydin and Jeglum, 2006).

2.4 Empirical Modeling Approaches

Three modeling approaches were combined to partition the LORCA and RERCA into millennial and decadal C fluxes, respectively (**Figure 3**).

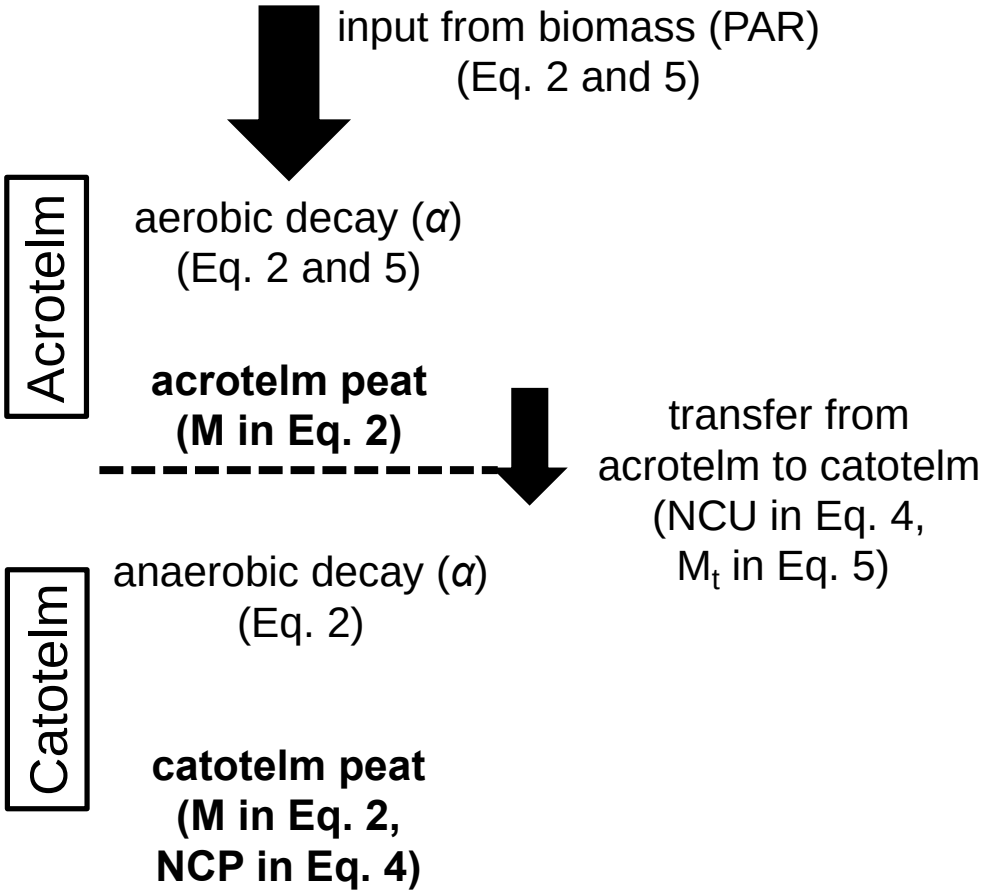

Figure 3 A diagram describing the empirical modelling approach. Peat is added to the acrotelm at a constant rate (PAR), and this mass (M) is decayed at a constant rate (α). This mass is transferred into the catotelm (M_t) at the acrotelm/catotelm boundary. The net carbon pool (NCP) in the catotelm is used to back-calculate the net carbon uptake (NCU) with an assumed carbon content of 50% and the net carbon release (NCR) from these values. This schematic (modified from Loisel and Yu, 2013a) describes the linkages between short- vs. long-term carbon accumulation in peatlands by forward-calculating peat decay in the acrotelm and back-calculating peat decay in the catotelm.

First, the exponential peat decay model (Clymo, 1984) was applied to the CM of each peat profile to tease apart its long-term peat addition rate (PAR) from its peat decay rate (α). This

model assumes that, over time (t), peat is added at a constant rate into the catotelm, while the growing peat deposit is also decaying at a constant rate that follows an exponential function, as shown in Equations 1 and 2 (derived from Clymo, 1984):

1. $\frac{dM}{dt} = PAR - \alpha * M$

   which has the analytical solution of

2. $M = \left(\frac{PAR}{\alpha}\right) * (1 - e^{-\alpha * t})$

I derived PAR and α for the catotelm (PAR_c, α_c) and acrotelm (PAR_α, α_α) separately using a curve fitting analysis in SigmaPlot (**Figure 3**). The catotelm values from each core were then fed to the peat C flux reconstruction model (Yu, 2011), while the acrotelm values were used to drive the peat decomposition model (PDM; Frolking et al., 2001).

The C flux reconstruction model, also known as the mega-bog approach (MBA), was used to estimate the net C uptake (NCU) and C release (NCR) terms from the catotelm (Loisel and Yu, 2013a; Packalen et al., 2014). The MBA (**Figure 3**) derives these uptake and release terms from the total C pool (obtained from peat core data) by back-calculating the initial amount of peat that reached the catotelm (C uptake) and modeling its subsequent long-term decomposition (C release), the latter being based on Clymo's decay coefficient (α_c). In these equations, any given peat cohort (*k)* is any section of the profile older than time *t*, and is used to define the boundaries for each measurement of the net C pool (NCP). Note that in this backward model, at any given *t*, the C release term includes decomposition from all peat cohorts that are older than *t*. This model uses Equations 3 and 4 (derived from Yu, 2011):

3. $NCU_t = \frac{NCP_t}{e^{-\alpha * t}}$

4. $NCR_t = \sum_{k=t}^{initiation\ age} \left(\frac{NCP_k}{e^{-\alpha * t}} - \frac{NCP_k}{e^{-\alpha * (t-1)}}\right)$

Lastly, the PDM (**Figure 3**) was used to simulate peat mass loss in the acrotelm over time. Here I simply assume that the initial peat mass M_0 in the acrotelm is equal to PAR_a, and that the initial decomposition rate k_0, which decreases as a function of peat mass loss over time, is equal to α_a. In a forward model, the peat mass then decreases following the exponential decay model over time (t), in years, as shown in Equation 5 (derived from Frolking et al., 2001):

5. $$M_t = \frac{M_0}{1+k_o t} = \frac{PAR}{1+\alpha * t}$$

Overall the residual peat mass at the "bottom" of the forward acrotelm model (from the PDM simulation) can be compared to the initial peat mass, or initial C uptake, at the "top" of the catotelm from the backward model (from the MBA simulation). This allows us to link short-term acrotelm dynamics to long-term catotelm C storage, by simulating how much peat C can be transferred into the catotelm in the future and how it compares to previous input rates (**Figure 3**).

The three modeling approaches were used to compare RERCA and LORCA values for sites BP and MP only. I selected those two cores because they were the only ones that met our criteria, i.e., they each have at least three ^{14}C dates near the surface and additional ^{14}C dates downcore.

2.5 Peat and Climate Data Synthesis

I compiled, synthesized, and analyzed 186 sites for the RERCA dataset (**Supplementary Table A1** and **A2**) from global peatlands. To be included in this dataset, sites needed to have at least 3 dates (e.g., ^{14}C, ^{210}Pb, tephra, etc.) to constrain the chronology of the past 150 years as well as bulk density data. Once these sites were selected, I calculated CM values for each core, similarly as described above for our own cores. CM values were obtained for 50, 100 and 150-year time steps so that incremental peat addition rates could be calculated.

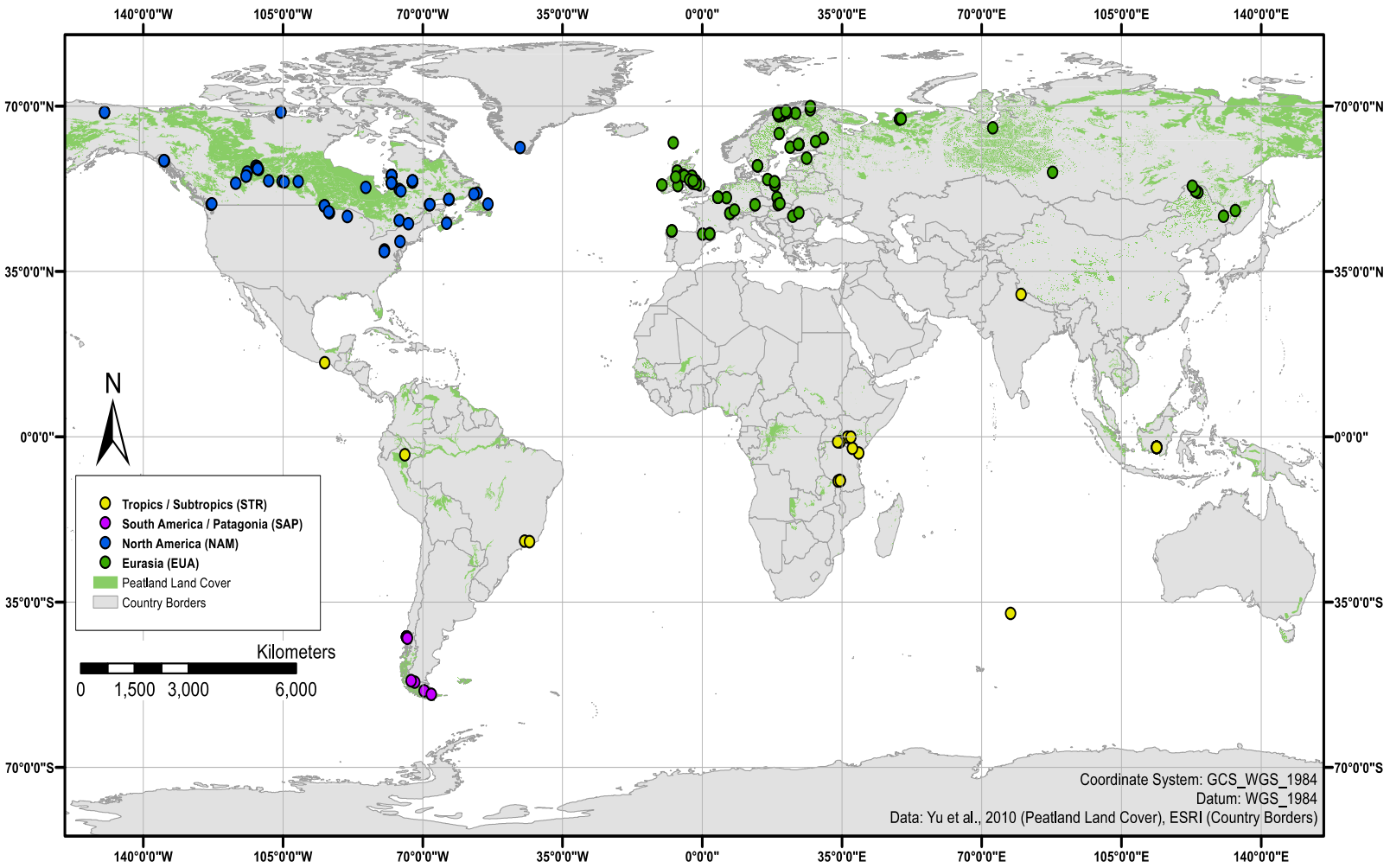

Figure 4 Global distribution of peatland sites included in the new RERCA database. Sites are divided into four geographic regions: North America (NAM; blue circles), Eurasia (EUA; green circles), South America/Patagonia (SAP; purple circles), and Tropics/Subtropics (STR; yellow circles). The global peatland land cover (green area) data was originally published in Yu et al. (2010).

I extracted climate data from the Climate Research Unit (CRU) database, version 2.0 (New et al., 2002) which includes gridded data for years 1961 to 1990. This global dataset covers all land areas (excluding Antarctica) and has a grid cell resolution of 10' x 10'. As peatlands are sensitive to both temperature and moisture parameters, I derived bioclimatic indices that would represent those two factors. The temperature variable I used is called "photosynthetically active radiation over the growing season (PAR0)", which measures the amount of light available for photosynthesis during the growing season (degree days > 0° C); the unit is mol photons/m^2/season. It can be understood as the plant C fixation potential during the growing seasons (Loisel et al., 2012) and is computed on the basis of incoming solar radiation, temperature, and cloudiness for any given grid cell (Prentice et al., 1993). The moisture index (MI) has the formula P/E_q, where P is annual precipitation and E_q is equilibrium evapotranspiration. It represents the moisture balance for any given grid cell, as obtained from precipitation vs. equilibrium evapotranspiration, which is based on solar radiation values (Prentice et al., 1993). These two indices were selected on the basis of previous work (Loisel et al., 2012; Charman et al., 2013; Gallego-Sala et al., 2018) who show that they adequately represent the hydroclimate regime of peatlands.

2.6 Statistical Analysis

The global RERCA database was divided into four geographic regions: North America (NAM), Eurasia (EUA), Tropics/Subtropics (STR), and South America/Patagonia (SAP). The cumulative peat mass values at 50, 100, and 150 years were compared across these regions using a 1-way analysis of variance (ANOVA); statistical significance was assessed using Tukey's HSD test. CM values were also plotted against the climate parameters, and a Pearson's regression test

was used in order to determine whether a statistically significant relationship existed between them.

3. RESULTS

3.1 Peat Geochemistry and Age-Depth Models

In the following paragraphs, I present the peat chronology for each core and outline the main geochemical information. As a reminder, water content (WC), organic matter content (OMC), bulk density (BD), and organic matter bulk density (OMBD) values were measured. Peat cumulative mass (CM) and peat-carbon accumulation rate (PCAR) were calculated based on the geochemical results.

General Findings On the basis of 1721 measurements, the average WC for all cores is 87.4 ± 10.2 (SD) % and the average OM content is 85.9 ± 20.6 % (**Table 3**). The average OMBD is 0.087 ± 0.026 g/cm^3, and the average BD is 0.126 ± 0.147 g/cm^3 (**Table 3**). The reported standard deviation statistics for these properties are high due to the inclusion of both mineral and peat sections. Total peat CM for each core (excluding SJ and CP2) averages 44.02 ± 18.37 g/cm^2. These geochemical properties are typical of ombrotrophic peatland ecosystems, where high organic matter content accumulates under mostly waterlogged conditions (Loisel et al., 2014; Loisel, 2015). Median peat inception age is 11,302 cal. BP, with the youngest inception age at 5,740 cal. BP (JB site) and the oldest at 15,590 cal. BP (BP site). Note that sites SJ, CP, FP, and RP were omitted from this analysis because we don't have basal dates for them. Average time-weighted PCAR (excluding SJ and CP2) is 23.21 ± 9.24 g C/m^2/yr, with high levels of variation found between, and within, each core (**Table 3**). In general, the A/D models exhibit linear to slightly convex shapes, with accumulation rates that generally increase over time (**Figure 5**). One notable exception is site PAN, with a concave shape.

Table 3 Summary statistics from peat geochemical properties for the new peat cores from southern Patagonia, South America. Averages and standard deviations include all cores, except those marked with an asterisk (*); the latter were excluded because the cores were incomplete.

Core	*Depth (cm)*	*Median Inception Age (cal. BP)*	*Average WC (%)*	*Average OMC (%)*	*Average BD (g/cc)*	*Average Organic Matter BD (g/cm^3)*	*Total Cumulative Mass at Peat Depth (g/cm^2)*	*Average PCAR ($gC/m^2/yr$)*	*Time-Weighted PCAR ($gC/m^2/yr$)*
BP	769	15547	87.7	88.4	0.124	0.095	72.89	12.03	23.17
PAN	515	11148	88.6	90.0	0.119	0.085	51.76	13.09	22.04
MP	409	13682	90.8	94.4	0.090	0.084	36.35	7.94	12.55
JB	569	5741	82.3	67.8	0.108	0.070	61.56	17.16	35.09
SJ	124*	-	92.5	94.7	0.075	0.071	9.32*	11.64	21.36*
CP2	399	10411	79.9	71.0	0.221	0.089	33.15*	8.06	16.35*
CP	249	-	87.2	90.3	0.121	0.094	23.02	-	-
FP	349	-	89.3	92.8	0.099	0.088	31.39	-	-
RP	299	-	85.7	88.6	0.138	0.095	31.16	-	-
Average	435	11302	87.4	85.9	0.126	0.087	44.02	12.97	23.21
Standard Deviation	174	4140	10.3	20.6	0.147	0.026	18.37	7.92	9.24
n	1736	1250	1721	1721	1721	1721	1736	1213	-

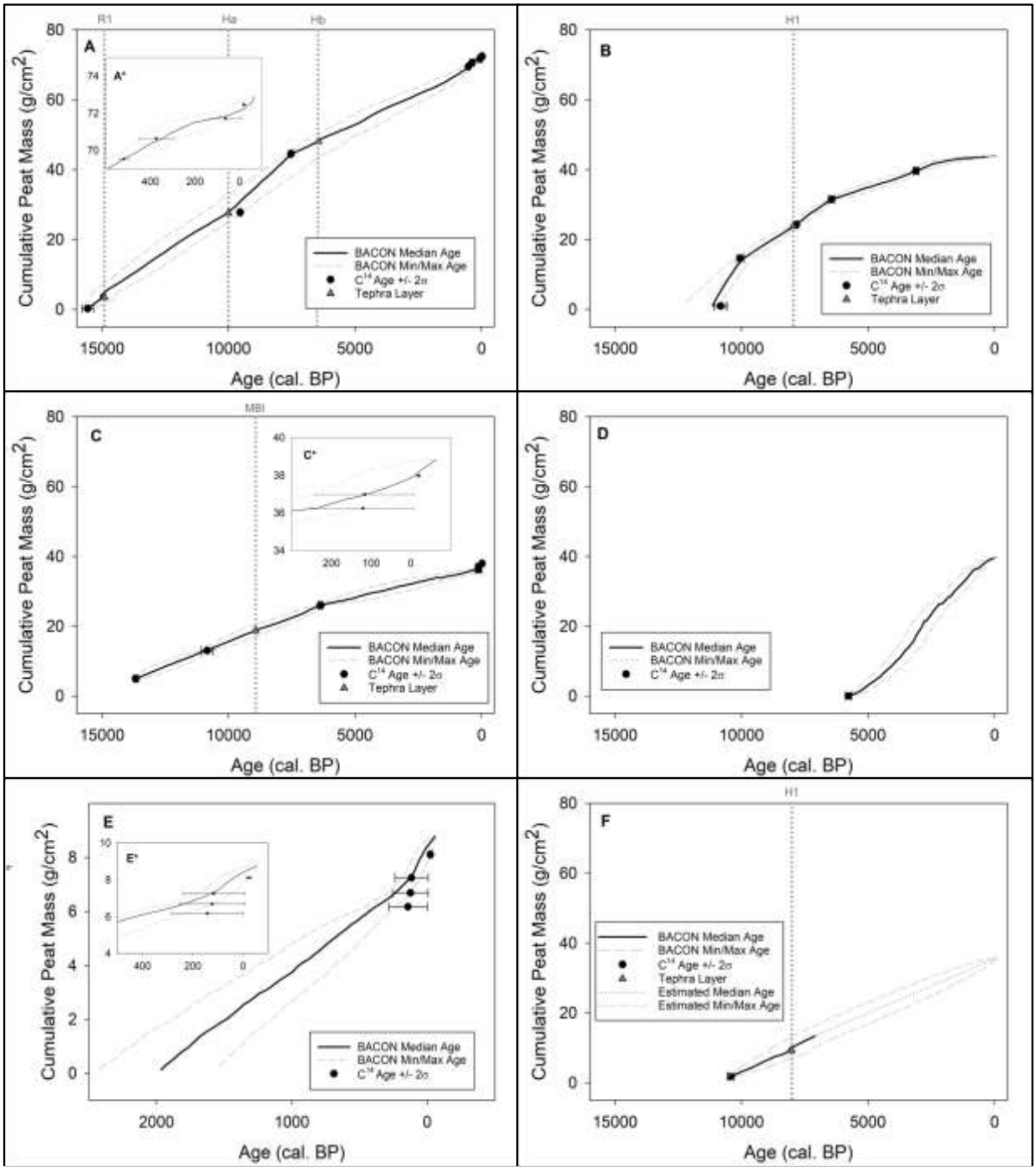

Figure 5 Age-depth models for the new peatland study sites from southern Patagonia. Cumulative peat mass (g/cm^2) is plotted against the median age (cal. BP, solid lines) that was obtained with Bacon (Blaauw and Christen, 2011); the 95% confidence interval is also shown (dashed lines). Age-depth models for complete cores: BP (A), PAN (B), MP (C), and JB (D), and incomplete cores: SJ (E) and CP2 (F) are presented. Inset graphs show recent age-depth curves for cores BP (A*), MP (C*), and SJ (E*). Median ^{14}C dates (black circles with 2 sigma range error bars) and volcanic ash layers (dark gray triangles and dotted lines; Supplementary Table A3) are presented.

BP Core Peat accumulation started at 15,590 ± 225 cal. BP atop a light brown, highly decomposed material. The average OMBD (0.09 g/cm^2) and time-weighted PCAR (23.17 gC/m^2/yr) are representative of the general trend in this core's development, except for a section of the core from approximately 10,000 to 8,000 cal. BP. This subsection is bounded by volcanic eruptions (Ha and Hb) and contains higher than average time-weighted PCAR (33.09 gC/m^2/yr), but the same average OMBD, indicating that those greater values were caused by rapid peat accumulation rather than by denser peat.

MP Core Peat accumulation started at 13,660 ± 96 cal. BP atop a clay-rich sediment layer containing small pieces of gravel and low silt content. The OMBD and PCAR rates of this core are uneven along the profile. During most of its developmental history (from ~ 14,000 to 5,000 cal. BP), this site was characterized by low variance in terms of its OMBD (mean = 0.081 g/cm^3, variance = 0.0002 g/cm^3), which was accompanied by a higher time-weighted PCAR (13.28 gC/m^2/yr). During the late Holocene (from ~ 5,000 to modern), this trend switches into a stage of greater variance and multiple oscillations (OMBD mean = 0.096 g/cm^3, variance = 0.0005 g/cm^3), accompanied by a lower time-weighted PCAR (8.78 gC/m^2/yr). These oscillations follow a step-like pattern, where gradual increases in OMBD are followed by abrupt decreases, each phase lasting approximately 1000 years (**Figure 6**).

PAN Core Peat accumulation started at 10,770 ± 242 cal. BP atop a sediment layer containing glacial clay and pebbles. The PAN core exhibits a step-like pattern in PCAR, separated into four subsections that gradually decrease in value over the development of the peatland. The average OMBD (0.09 g/cm^3) and time-weighted PCAR (22.04 gC/m^2/yr) underestimate the initial developmental stage of the peat profile (from ~ 11,000 to 10,000 cal. BP), where the OMBD (0.11 g/cm^3) and time-weighted PCAR (51.55 gC/m^2/yr) were much

higher. The following three sections of the core, lasting approximately ~ 3,000 - 4,000 years each (from ~10,000 cal. BP to modern), exhibit steadily decreasing OMBD (from 0.08 to 0.07 g/cm^3) and time-weighted PCAR (from 22.78 to 6.3 $gC/m^2/yr$) values.

JB Core Peat accumulation started at 5,740 ± 121 cal. BP, atop a clay-rich sediment layer. Since this core chronology is constrained by a single ^{14}C date, PCAR closely follows OMBD. Average OMBD (0.07 g/cm^3) and time-weighted PCAR (35.09 $gC/m^2/yr$) are retained throughout the peat core with relatively low variance, except for a peak at approximately 3,000 cal. BP (0.20 g/cm^3; 52.75 $gC/m^2/yr$), which is contemporaneous with the Aguilera volcanic eruption (3369 – 2863 cal. BP; Stern, 2008).

SJ and CP2 Cores I do not know when peat accumulation started at the SJ site, as we only retrieved a partial (non-basal) core. The average OMBD (0.07 g/cm^3) and time-weighted PCAR (21.36 $gC/m^2/yr$) for SJ do not exhibit any anomalies, and no further analyses or calculations were performed. In the case of CP2, peat accumulation started at 10,440 ± 137 cal. BP. Average OMBD (0.09 g/cm^3) and time-weighted PCAR (16.35 $gC/m^2/yr$) typically follow the averages, except for a peak in BD at approximately 8,000 cal. BP. This peak is followed by slight increases in OMBD and PCAR, but the most recent histories cannot be accessed due to having only kept the lower section of the core (375-250 cm).

CP1, FP, and RP Cores I obtained geochemical properties for the three remaining cores, though these were not ^{14}C-dated. Each core contains similar trends in OMBD, gradually decreasing towards the near surface, and an average ranging between 0.08 and 0.09 g/cm^3. For visual aid, I identified potential volcanic eruptions along these cores (**Figure 6**), though it is important to note that these cannot be validated due to a lack of dates.

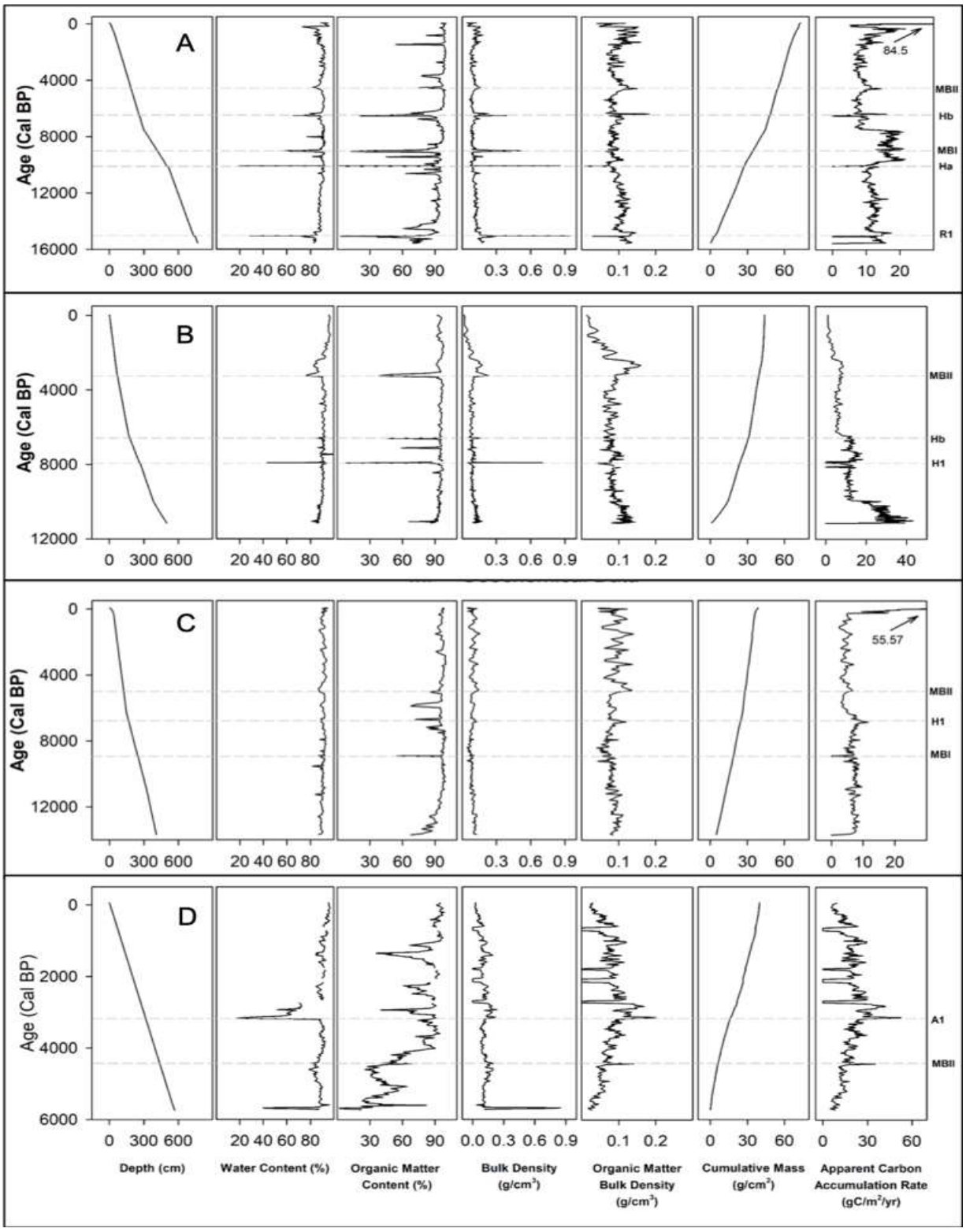

Figure 6 Peat geochemical data for southern Patagonian cores. For cores BP (A), PAN (B), MP (C), JB (D), SJ (E), and CP2 (F), results are plotted against ages (cal. BP) obtained from Bacon (see Figure 5). For cores CP (G), FP (H), and RP (I), which were not dated, geochemical data are plotted against peat depth. Volcanic ash layers (tephra) are included in each graph for reference (see Supplementary Table A3).

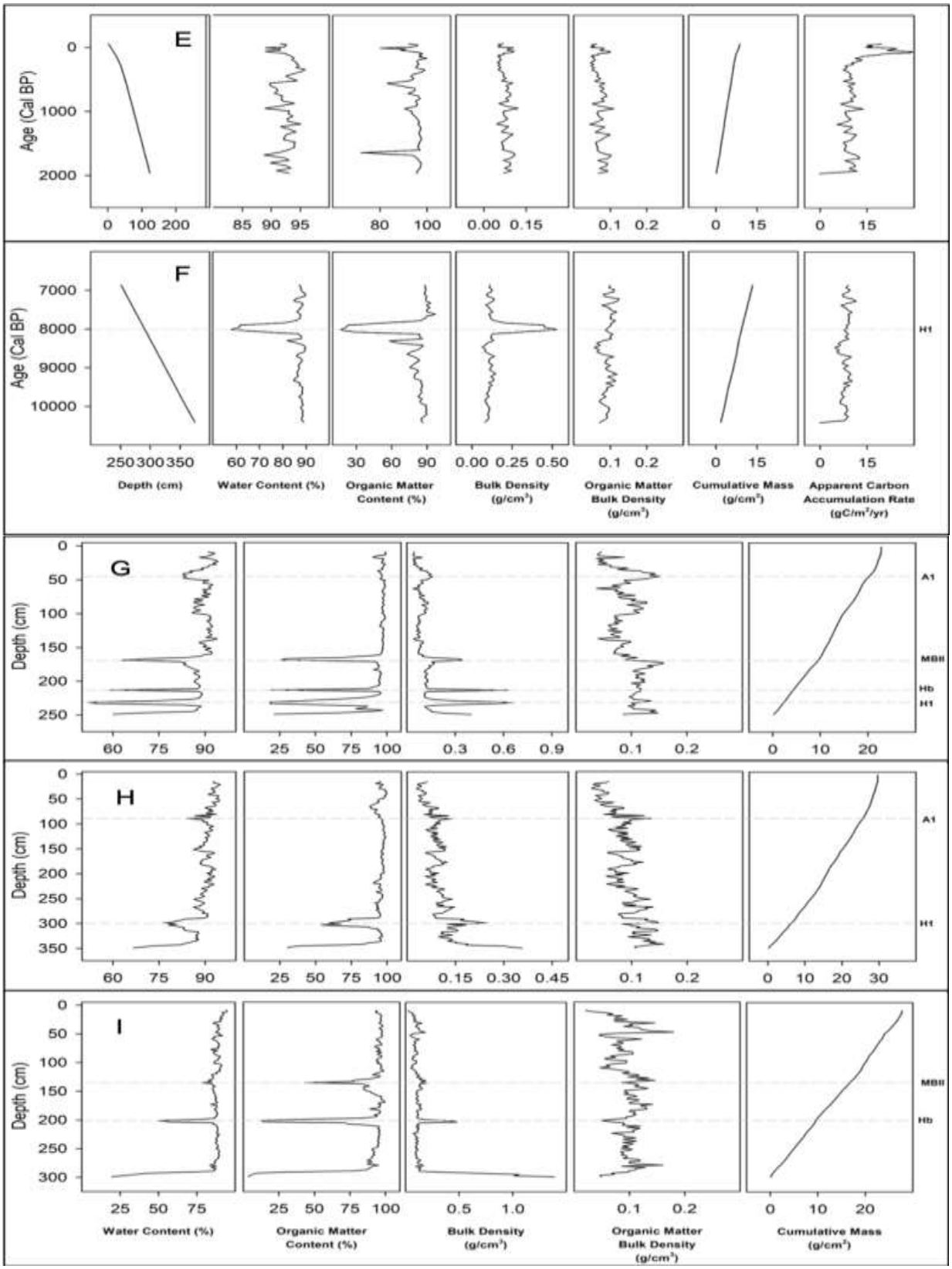

Figure 6 Continued

Tephra Identification Peaks in OMBD and BD were observed at several points along core profiles; when combined with glass shards, they indicate volcanic tephra layers (**Figure 6**). The depth and associated age of these layers was cross-referenced with median age calculations from the literature to determine which volcanic eruptions were present along the peat profiles (Kilian et al., 2006; Stern, 2008). Further analysis of these volcanic layers being beyond the scope of this paper, I won't discuss those here. Additional information concerning tephra methodology and analysis can be found in the Supplementary Information (Appendix A: **Supplementary Table A3**). Non-visible tephra layers (indicated only through geochemical anomalies) were included in the geochemical graphs (**Figure 6**) as a reference, but their provenance has not been confirmed through chemical fingerprinting at this time.

3.2 Peat Accumulation Models

Exponential Decay Model I utilized the exponential decay model (Clymo, 1984) to calculate peat addition rate (PAR) and decomposition coefficient (α) for each core. As a reminder, those two parameters are assumed to remain constant through time (see section 2.4). The reported PAR and α parameters for the catotelm of core BP are 43 g OM/m^2/yr and 0.00005 /yr. For core MP, those values are 30 g OM/m^2/yr and 0.00001 /yr. These results can be understood as follows: the rate of peat transfer into the catotelm is greater for core BP (43 vs. 30 g OM/m^2/yr), and the decay coefficient is also greater for core BP (0.00005 vs. 0.00001 /yr). In other words, core BP sees a more rapid peat addition rate (yielding an overall thicker peat deposit) but it is also accompanied by faster decomposition (yielding an overall more concave peat accumulation profile; **Figure 5**). The values for cores BP and MP compare well with those from the region (Loisel and Yu, 2013b). I also calculated these parameters for the acrotelm

portions of the cores. For core BP, PAR and α were 221 g OM/m^2/yr and 0.0139 /yr, and 205 g OM/m^2/yr and 0.0073 /yr for core MP. As expected, the acrotelm PAR values are an order of magnitude greater than those for the catotelm, whereas the decay parameters are two to three orders of magnitude greater; this portion of the profile is where the bulk of peat diagenesis occurs (Clymo, 1965).

Mega-Bog Approach The peat-C flux reconstruction model (Yu, 2011), or the mega-bog approach (MBA), utilized the PAR and α from the catotelm to produce the net carbon pool (NCP), the net carbon uptake (NCU), and the net carbon release (NCR) for the catotelm of a peat core (see section 2.4 for details). The average NCU for cores BP and MP is 70.4 g OM/m^2/yr and 25.7 g OM/m^2/yr, respectively (**Figure 7**). It should come as no surprise that core BP has experienced greater C uptake than core MP throughout its history, given its thicker peat deposit and PAR value. For site BP, NCU is highest during the late Pleistocene, from 15,000 to 13,000 cal. BP, with an average of 50.8 g C/m^2/yr (or 101.6 g OM/m^2/yr), followed by a decreasing trend until 10,000 cal. BP, where it reaches 39.9 g C/m^2/yr. The period between 10,000 and 8,000 cal. BP sees an increase in NCU (up to 54.5 g C/m^2/yr), followed by low values until modern-day that oscillate between 17.1 and 33.8 g C/m^2/yr (**Figure 7**). In general, this pattern describes rapid C sequestration during the first half of the peatland's developmental history, followed by a substantial decrease in its C-sink function since the mid Holocene. Site MP displays a similar story, with greatest NCU during its early developmental phase (13,000 to 10,000 cal. BP), followed by a dip in C uptake until 8,000 cal. BP, followed by low values until modern-day (**Figure 7**). That said, the accrued C reservoir of site MP has been much lower than that of BP.

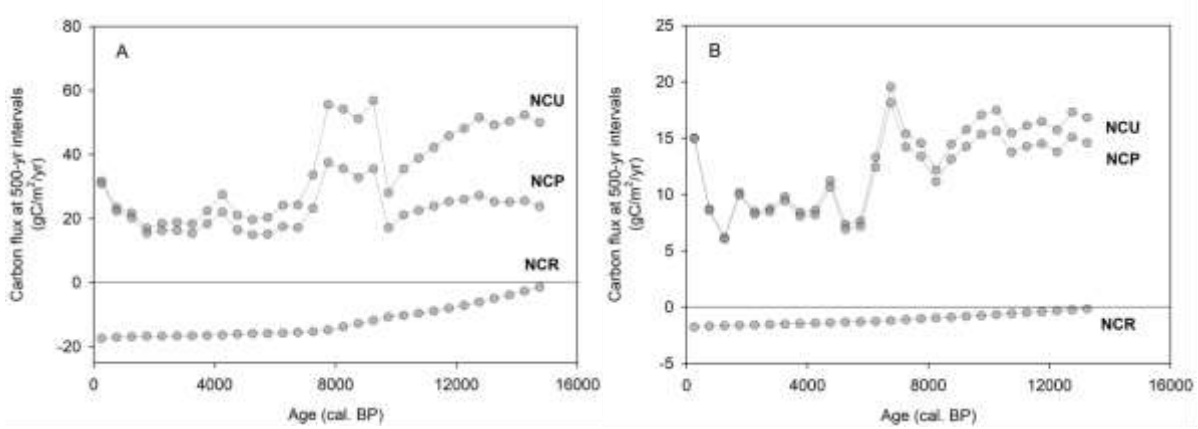

Figure 7 Peat carbon flux reconstruction models. The developmental history of cores BP (A) and MP (B), broken up into 500yr intervals (cohorts), are presented. The net carbon pool (NCP; derived from Equations 3 and 4) shows the current C stock of the core as measured along the peat cores. The net carbon uptake (NCU) represents the average C that was added to the catotelm within each cohort, and the net carbon release (NCR) is the summed release of C from the catotelm over the lifespan of each core.

Peat Decomposition Model The Peat Decomposition Model (PDM; Frolking et al., 2001) predicts peat mass loss through the acrotelm profile, such that the remaining mass at the base of the acrotelm would be transferred to the catotelm (see section 2.4 for details). After decomposing the acrotelm peat for 300 years, the remaining peat mass in the acrotelm for core BP was 42.69 g OM/m^2/yr, vs. 64.19 g OM/m^2/yr for core MP. In this case, despite site BP having a greater input value (PAR = 221 g OM/m^2/yr), site MP is expected to transfer more peat to the catotelm. This is likely because it appears to be decomposing at a much slower rate than BP (decay parameter for MP = 0.0073 /yr vs. BP = 0.0139 /yr).

The "top of catotelm" NCU can be compared to the "bottom of acrotelm" remaining peat mass, as they both reflect the amount of peat transferred from the acrotelm to the catotelm. Our results suggest that, in the case of core BP, the long-term NCU (70.4 g OM/m^2/yr) is significantly greater than the bottom of acrotelm peat mass (42.69 g OM/m^2/yr), suggesting that the current acrotelm is unlikely to support the long-term C sink capacity for this site. Conversely,

in the case of core MP, the long-term NCU (25.86 g OM/m^2/yr) is significantly smaller than the bottom of acrotelm peat mass (64.19 g OM/m^2/yr), suggesting that this site should see an increase in its long-term C storage capacity.

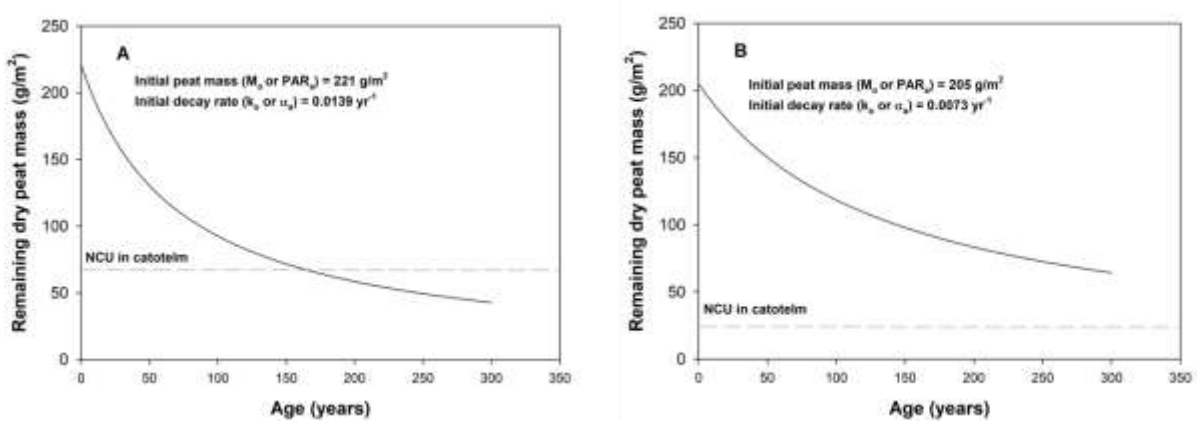

Figure 8 Recent rates of peat decomposition within the acrotelm for cores BP (A) and MP (B). The initial peat addition rate (PAR_a) and decay coefficient (α_a) were used to calculate peat mass loss (black line) over 300 years (Frolking et al., 2001; Equation 5). The NCU (dashed line; multiplied by 2 to convert C mass into peat OM mass for direct comparison) was derived from the mega-bog approach (Yu, 2011; Figure 7) and used to identify potential shifts in the rate of C transfer from the acrotelm and catotelm over time.

3.3 Global Recent Rates of Carbon Accumulation

Cumulative peat mass was calculated at 50, 100, and 150 years since coring (CM 50-100-150) for each site included in the global RERCA database. The overall mean values for CM 50-100-150 is 1.37 g/cm^2, 2.08 g/cm^2, and 2.59 g/cm^2, respectively. The range of values is 0.11 – 10.2 g/cm^2 for CM50, 0.19 – 14.7 g/cm^2 for CM100, and 0.24 – 22.9 g/cm^2 for CM150. Mean, minimum, and maximum CM values for each region can be found in **Table 4**. Notably, Tukey's HSD post-hoc test (**Table 5**) from the ANOVA revealed that only the STR region was characterized by mean CM 50-100-150 values that were significantly different than any other region ($p < 0.0001$). While SAP was characterized by the lowest CM values, this difference was

not significantly different when compared to NAM and EUA ($p > 0.64$ and $p > 0.56$, respectively; **Figure 9**).

Table 4 Summary statistics and average recent rates of carbon accumulation (RERCA). Table compares cumulative peat mass (CM) after 50, 100, and 150 years and RERCA for each region.

Region	*Minimum (g/cm^2)*	*Median (g/cm^2)*	*Maximum (g/cm^2)*	*Standard Deviation (g/cm^2)*	*RERCA ($gC/m^2/yr$)*
CM50					
EUA	0.21	1.13	3.26	0.59	114.85
NAM	0.11	1.15	6.52	0.87	113.32
SAP	0.49	0.68	0.88	0.14	68.31
STR	0.31	2.96	10.19	2.50	296.04
CM100					
EUA	0.43	1.69	5.18	0.79	91.07
NAM	0.19	1.82	8.79	1.44	84.51
SAP	0.78	1.08	1.42	0.21	53.83
STR	0.38	4.27	14.70	3.70	213.37
CM150					
EUA	0.70	2.10	6.42	0.97	74.78
NAM	0.24	2.24	9.76	1.74	69.86
SAP	0.99	1.41	1.86	0.34	46.97
STR	0.46	5.44	22.87	5.20	181.28

Table 5 Results from Tukey's HSD post-hoc test performed on a one-way analysis of variance (ANOVA). Table shows the relationship between cumulative peat mass (CM) after 50, 100, and 150 years of accumulation across the four study regions. NAM: North America; EUA: Eurasia; SAP: South America/Patagonia; STR: Subtropics/Tropics.

	Tukey's HSD p-value		
Region	*CM50*	*CM100*	*CM150*
NAM-EUA	0.9997975	0.9666673	0.9798511
SAP-EUA	0.6078121	0.5678477	0.7011440
STR-EUA	< 0.000001	< 0.000001	< 0.000001
SAP-NAM	0.6429065	0.7185739	0.8155925
STR-NAM	< 0.000001	< 0.000001	< 0.000001
STR-SAP	0.0000002	0.0000018	0.0000078

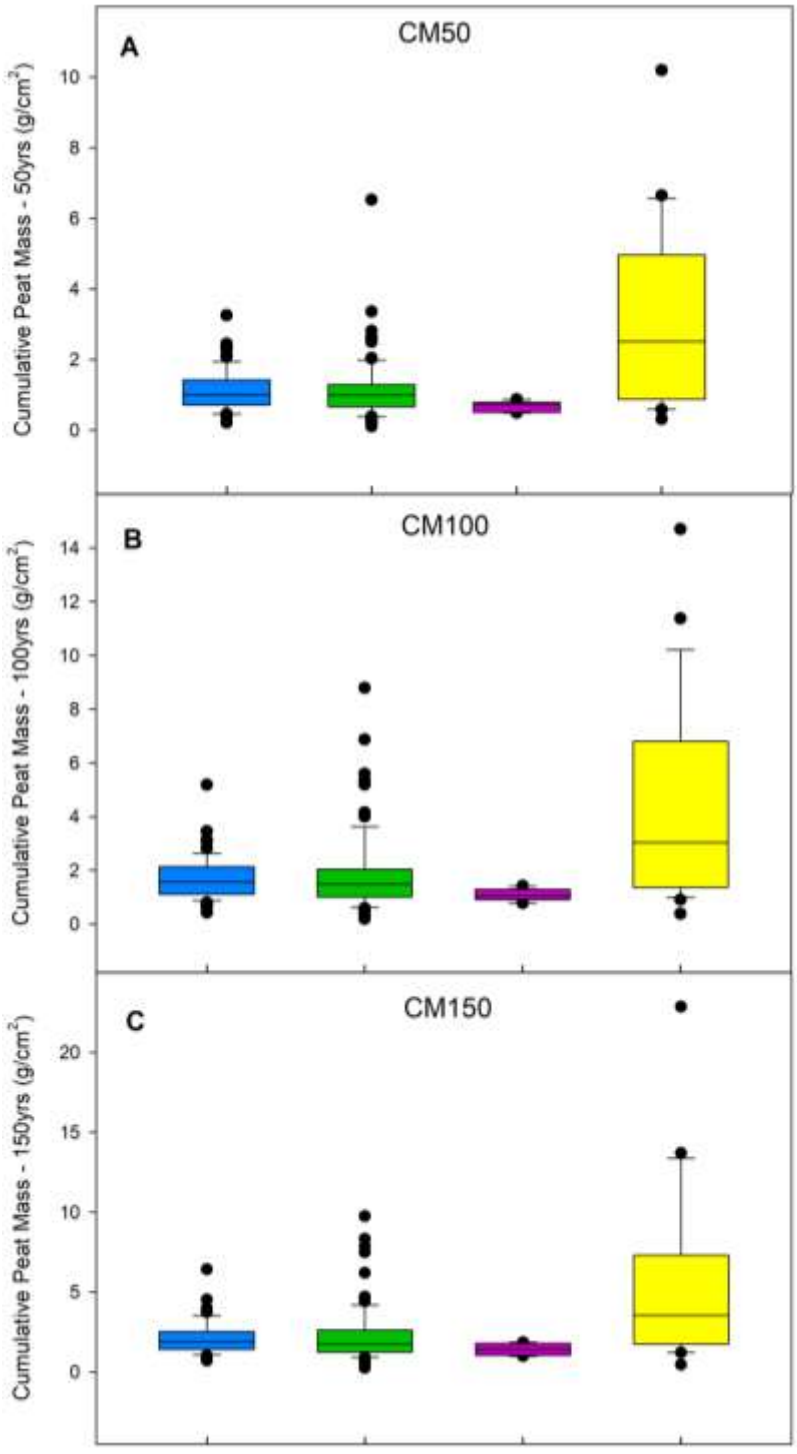

Figure 9 Recent cumulative peat mass (CM) from sites worldwide (n = 186) after 50 (A), 100 (B), and 150 (C) years. The data are presented by region: North America (NAM; blue), Eurasia (EUA; green), South America/Patagonia (SAP; purple), and Tropics/Subtropics (STR; yellow). Each box-plot with whiskers displays the sample median (central line), 25th and 75th percentiles (boxes), 10th and 90th percentiles (whiskers), and 5th and 95th percentiles (closed circles).

In terms of the influence of climate, PAR0 was strongly positively correlated with recent CM (Pearson's $R^2 > 0.54$; **Figure 10**). Interestingly, the relationship was strongest with CM50 ($R^2 = 0.54$, and decreased as time went by ($R^2 = 0.48$ for CM100 and 0.45 for CM150). Over time, CM indeed becomes less strongly correlated with PAR0, as indicated by the lowering slopes and correlation coefficients. This is likely due to decomposition processes becoming more important in the long run (i.e., the primary role of temperature on peat formation gets replaced by the primary role of peat decay over time; **Figure 10**). In terms of moisture, MI was negatively correlated with CM (Pearsons's $R^2 > -0.27$; **Figure 11**), with the highest correlation with CM50 ($R^2 = -0.34$), decreasing as time went by ($R^2 = -0.30$ for CM100 and -0.27 for CM150). As previously mentioned, MI measures the amount of precipitation over equilibrium evapotranspiration based on net radiation. Sites in warm climates with relatively high precipitation would experience MI values closer to one (because P may approach E_q), whereas sites with lower precipitation in cooler climates could yield a higher MI due to a greater difference between P and E_q. Although it would seem that peatland C sequestration would be greater in areas with a higher MI, our results indicate that this parameter does not exhibit a strong control on short-term C accumulation. This may be due to other factors affecting moisture conditions in a peatland, beyond P and E_q, such as local groundwater inputs. Seasonal trends in P vs. E_q could also be analyzed in greater detail.

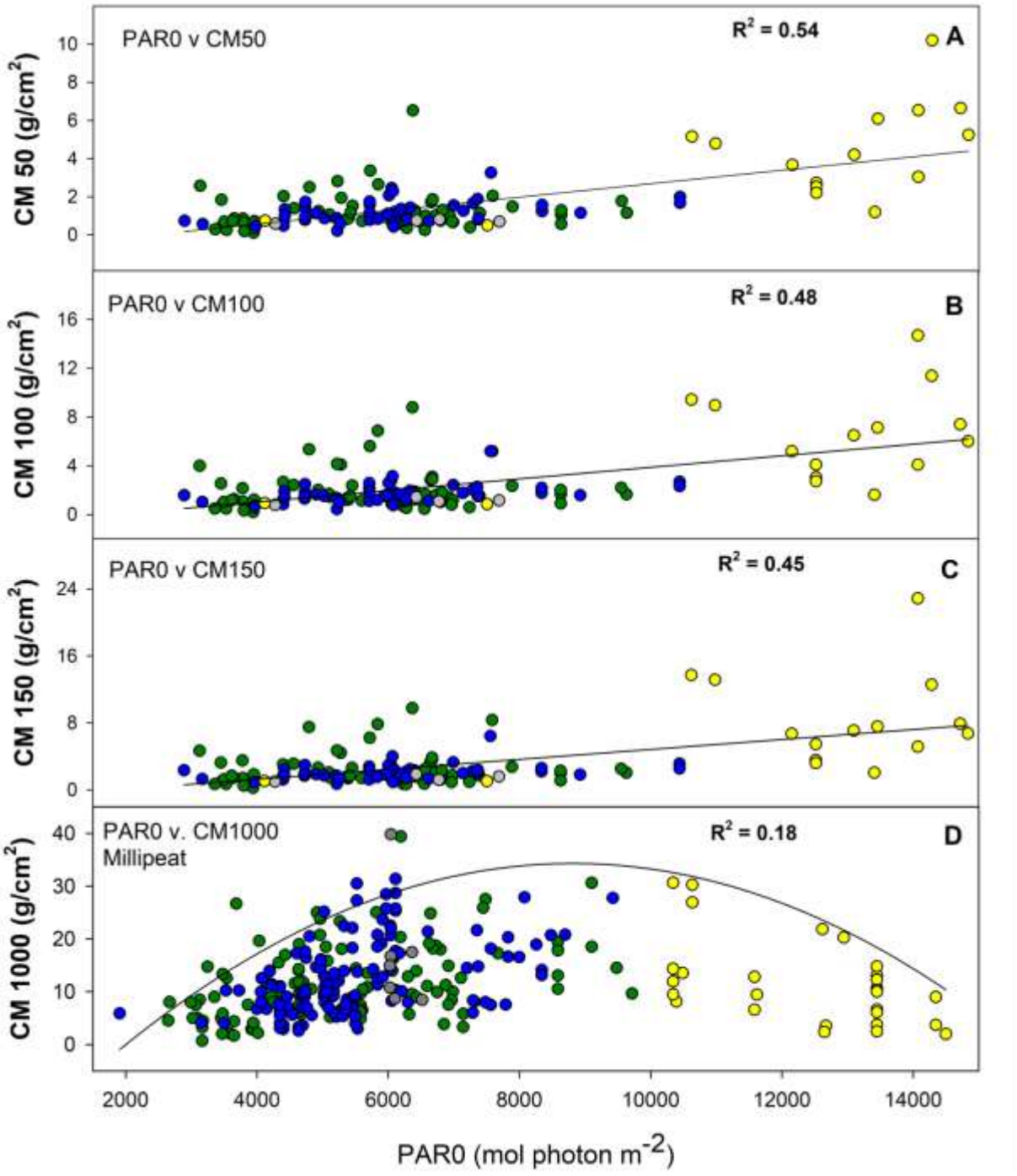

Figure 10 Photosynthetically active radiation integrated over the growing season (PAR0) in relation with recent cumulative peat mass (CM) after 50 (A), 100 (B), 150 (C), and 1000 (D) years. Note that for panel (D), the time interval used was 850-1850 AD to avoid the short-term acrotelm dynamics and focus on long-term carbon accumulation. Pearson's correlation coefficients (R^2) are shown for each dataset, demonstrating a weakening correlation as peat ages (see Supplementary Table A1 and A2 for details). Data for panel D come from Gallego-Sala et al. (2018); see section 3.3.

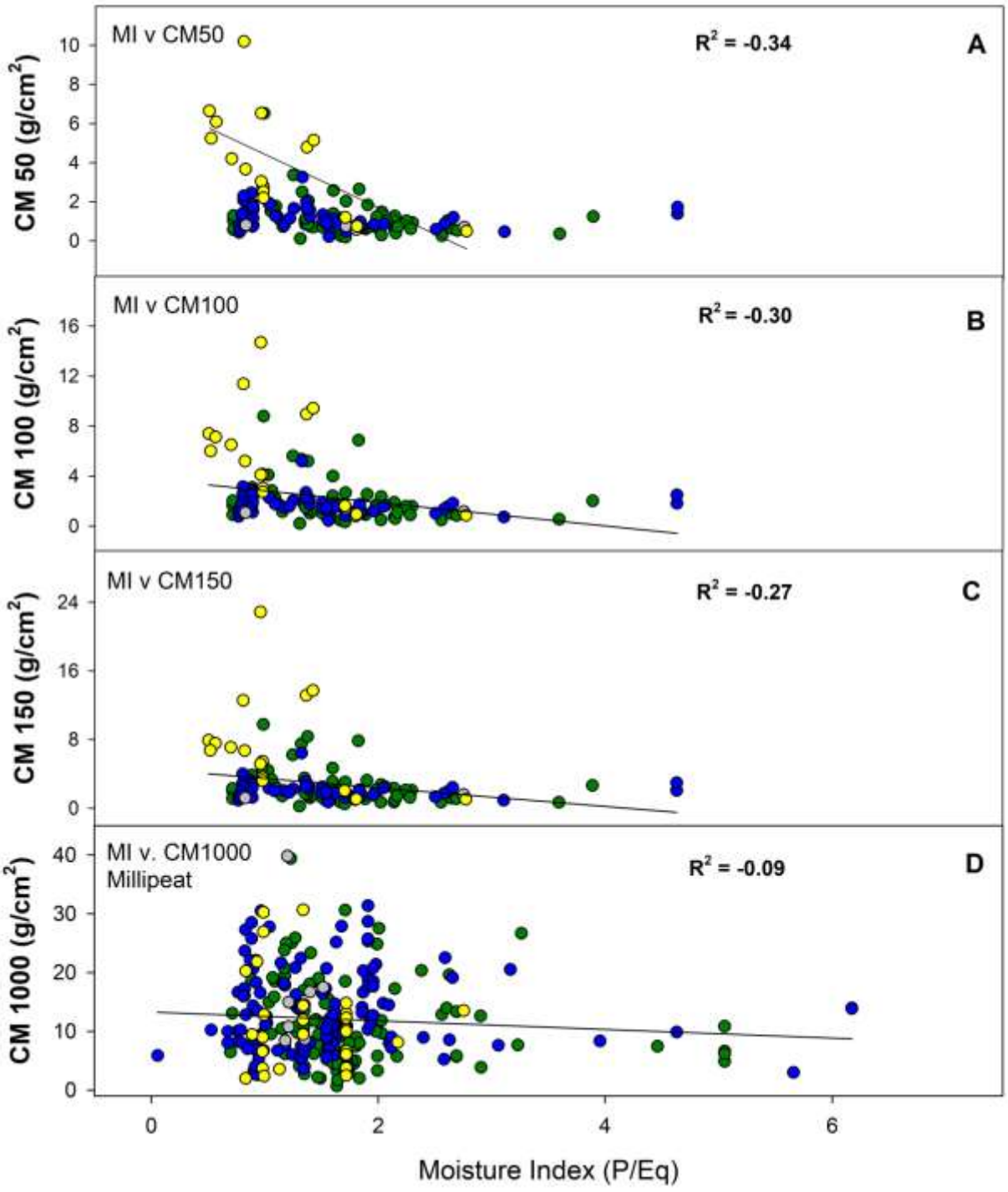

Figure 11 Moisture Index (MI) in relation with cumulative peat mass (CM) after 50 (A), 100 (B), 150 (C), and 1000 (D) years. Pearson's correlation coefficients (R^2) are shown for each dataset, demonstrating a weakening correlation as peat ages (see Supplementary Table A1 and A2 for details). Data for panel D come from Gallego-Sala et al. (2018); see Figure 10 and section 3.3.

4. DISCUSSION

4.1 Long-Term Carbon Accumulation in Patagonia Peatlands

On the basis of the nine peat cores analyzed in this study, I find that, across mainland SSA, peatlands have been accumulating C since approximately 16,000 cal. BP. This finding is corroborated by other studies, including a literature review containing 53 sites that shows a minimum inception time of ~ 17,000 cal. BP and a mean inception age of 12,370 cal. BP (Loisel, 2015). Across this region, the spatial and temporal pattern of peatland initiation follows regional deglaciation and associated land availability, as well as deglacial warming conditions. McCulloch and Davies (2001) conducted a paleoenvironmental analysis on a peat core from the southern Patagonian region, indicating glacial retreat just south of Punta Arenas at Puerto del Hambre (53.6°S, 70.9°W) as far back as 17,330 cal. BP, and a subsequent rapid deglaciation in a northwestern pattern, towards the Southern Patagonian Ice Field, where the ice sheet originated. In Tierra del Fuego, peat initiation occurred during the early Holocene, with my oldest core dating back to 11,150 cal. BP. McCulloch et al. (2019) conducted paleoenvironmental analysis on the lacustrine mud found at the bottom of a peat core from Navarino Island (54.93°S, 67.35°W), and found that while glacial retreat began around 16,200 cal. BP in this region, cool conditions persisted throughout the glacial period into the early Holocene at approximately 12,390 cal. BP. These findings further support the delayed peat inception seen in our own cores.

In terms of C sequestration, my results confirm that Patagonian peatlands are effective long-term land C reservoirs. Mean soil C density (kg C/m^2), which is quantified here as the product of mean organic C density and mean peat thickness, yields an averaged Patagonian peat

C density value of 197 ± 83 kg C/m^2, with a minimum of 114 kg C/m^2 (CP site) and a maximum of 365 kg C/m^2 (BP site). This new average is higher than, but within the error range of, a previous estimate of 154 ± 11 kg C/m^2 that was based on 42 sites (Loisel, 2015). In a study conducted by Peri et al. (2018), in the Santa Cruz Province in southern Patagonia, the total soil organic carbon (SOC) content (top 30cm) ranged from 1.38 to 32.63 kg C/m^2. They found variation in SOC to be correlated with vegetation types, reporting differences amongst shrubs (3.8 - 5.5 kg C/m^2), grasslands (5.9 - 6.8 kg C/m^2), and forests (12.1 - 12.3 kg C/m^2), further indicating the effectiveness of peatland C sequestration when compared to other regional ecosystems. Patagonian peatland C content is in line with previous estimates for northern high latitudes, which range between 55 kg C/m^2 (Turunen et al., 2002) and 180 kg C/m^2 (Sheng et al., 2004).

Long-term C accumulation rates (LORCA) for my cores exhibit spatial and temporal patterns that can be tied to the regional climate. In the early Holocene (~ 10,500 to 7,500 cal. BP), our four oldest cores (BP, MP, PAN, and CP2) exhibit elevated PCAR, likely due to the onset of warmer conditions that persisted throughout this period (Moreno et al., 2018), which is also characterized by smaller glaciers following rapid deglaciation (Strelin et al., 2014; Kaplan et al., 2016). Beginning at approximately 7,500 cal. BP, these same cores all experienced a decrease in PCAR; this peat accumulation slowdown is synchronous with a climate deterioration towards cooler conditions that persisted until ~ 4,200 cal. BP. These cooler conditions also led to glacial expansion across the Southern Patagonian Ice Sheet, as indicated by mean moraine ages based on ^{10}Be and ^{14}C ages (Strelin et al., 2011; 2014). The first portion of the late Holocene (~ 4,200 to 2,500 cal. BP) was characterized by warmer and drier conditions (Moreno et al., 2014; 2018), leading to increased PCAR in BP and MP, and increased OMBD in four of our cores (BP,

MP, PAN, and JB). In core MP, this time period is also characterized by multi-centennial-scale fluctuations in OMBD; a similar pattern was observed in a core described in Loisel and Yu (2013c); these fluctuations could relate to an increase in the westerly variability, also suggested by Moreno et al. (2009) on the basis of a pollen record from Lago Argentino. This was followed by a cooler and/or wetter period (~2,200 to 400 cal. BP; Moreno et al., 2018) during which there was a decrease in OMBD for five of our cores (BP, MP, PAN, JB, and SJ); similar fluctuations persisted during this time period as well (Moreno et al., 2009; Loisel and Yu, 2013c).

This study also provides a number of new findings as well as information on areas previously understudied. In mainland Chile, MP is located west of Puerto Natales on an isolated peninsula (Antonio Varas) from a region that does not appear to have been previously studied for peat. Likewise, JB is located just south of Torres del Paine National Park limits; to our knowledge, it is the farthest north a peat bog has ever been reported or studied in southern Patagonia. On Isla Grande, Tierra del Fuego, my sites provide much needed information from an area that is peatland-rich, but that remains largely understudied to this day (but see van Bellen et al., 2016; Xia et al., 2018). Our multiple sites, their ^{14}C dating, and geochemical properties will be useful in determining the C stock of this unique area. In concert with the Karukinka park rangers and the Chilean staff of the Wildlife Conservation Society, our team is working towards the creation of the first Carbon Conservation Park. The quantification of Karukinka's C reservoir will rely heavily on the cores described in this thesis.

4.2 Recent Carbon Accumulation in Patagonia Peatlands

Recent cumulative peat mass (CM) values for both BP and MP are within the range of observed values from other South-American/Patagonian (SAP) sites (**Table 4**). This low variance across the 10 sites reported here (2 from this study and 8 from the literature) may be due

to the low number of observations. However, the relatively small geographic range (i.e., latitudinal constraints) for this region may also contribute to low variance. In general, these recent CM values indicate that healthy peat accumulation is occurring across the region. That said, these net C addition rates in the near-surface peat cannot be directly compared with long-term rates from deeper layers. Indeed, a peatland could undergo net C loss, even though the uppermost part of the profile shows an apparent net gain.

To remediate this issue, a three-pronged modeling exercise was completed. The results reveal different peat accumulation histories for sites BP and MP. Despite these sites having similar acrotelm peat addition rates (221 vs. 205 g OM/m^2, respectively), they display different decomposition coefficients (0.0139 vs. 0.0073 /yr), with the latter being much lower than the former. Our empirical modeling approach (**Figure 8**) suggests that recent C accumulation in the acrotelm at site BP (more arid) will transfer less peat to the catotelm than what this site has been getting during most of its developmental history. This suggests that long-term peat accumulation is expected to slow down in the future at this site. Conversely, site MP (more oceanic) is predicted to increase its long-term C storage, as the peat addition rate into the catotelm is expected to increase given the acrotelm parameters. As explained in section 3.2, an increase in long-term peat accumulation rate is expected if the remaining peat mass at the bottom of the acrotelm is greater than the NCU values estimated from the catotelm, as is the case for MP. The reverse is true in the case of BP, where the remaining peat mass at the bottom of the acrotelm is smaller than the NCU in the catotelm.

Local climatic conditions are important factors controlling ecosystem development and plant communities. Site MP (51.75°S, 72.85°W) experiences high annual precipitation (1000 - 2000 mm/yr; **Figure 12**) and is located the furthest west of all our cores. The conifer

Pilgerodendron uviferum was found at this site and confirms the local humid climate. Meanwhile, site BP (52.06°S, 71.94°W) is located further east and experiences lower annual precipitation (500 - 1000 mm/yr; **Figure 12**); it is surrounded by deciduous tree *Nothofagus antarctica*, which is typically found in drier climates with milder temperatures (Peri et al., 2006). Located slightly farther east than BP is peatland site Rio Rubens (52.14°S, 71.88°W), which is the easternmost peat bog from the region; this site is characterized by even lower annual precipitation (450 to 650 mm/yr) and populated by *Nothofagus antarctica* (Huber and Markgraf, 2003). The steep west to east gradient of decreasing precipitation is mirrored in the vegetation found at our sites, and may explain the recent increase in C accumulation at BP vs. MP.

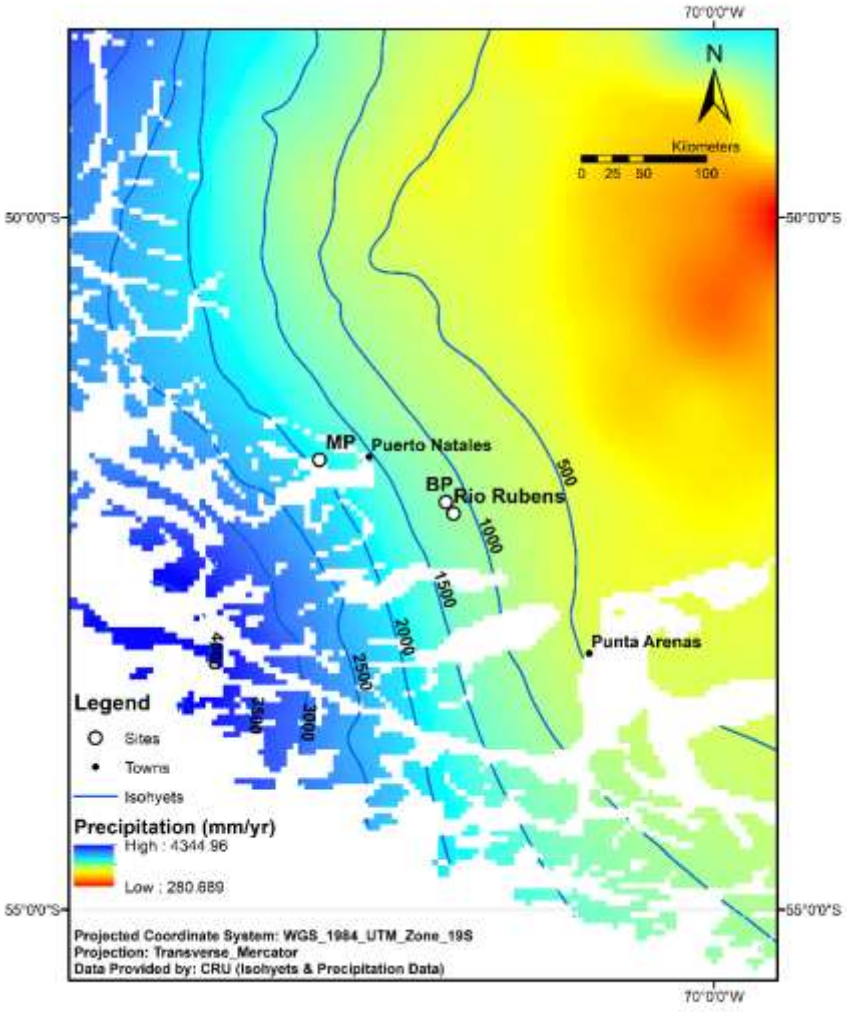

Figure 12 Peatland site distribution in southern Patagonia in relation to isohyets, reprinted from Lamy et al. (2010).

The modeling approach used in this study has been tested in Alaska (Loisel and Yu, 2013b) and against a peat accumulation model (Young et al., 2019). To date, it is considered the most honest and sole appropriate approach to link short- and long-term peat accumulation histories (Young et al., 2019). The unique combination of forward calculating peat decomposition in the acrotelm (PDM; Frolking et al., 2001) and back-calculating the C uptake from the catotelm (MBA; Yu, 2011) allows the researcher to compare these data from a common baseline (acrotelm/catotelm boundary). The outstanding limitations of this method are: (1) the

identification of the acrotelm/catotelm boundary along the real peat cores, as this boundary then influences the calculations of both the acrotelm and catotelm terms, and (2) the determination of the number of years peat should "decay" in the acrotelm before it gets transferred into the catotelm, also obviously influencing the "bottom of acrotelm" remaining peat mass value. These limitations could be addressed through the testing of multiple scenarios. For example, a sensitivity analysis could be conducted to test different acrotelm/catotelm depths. Likewise, one could decompose the acrotelm peat for different periods of time (e.g., 100, 200, 300, 400, and 500 years) to provide further insight into the sensitivity of the numbers selected. In my case, I selected 300 years as a conservative number; most studies suggest that acrotelm peat gets transferred to the catotelm after 100-200 years (Rydin and Jeglum, 2006).

4.3 Recent Rates of Carbon Accumulation Regionally vs. Across the Globe

The South American/Patagonian (SAP) sites are characterized by the lowest mean cumulative peat mass value between all regions (0.68 ± 0.14 g OM/cm^2 for CM50; 1.08 ± 0.21 g OM/cm^2 for CM100; 1.41 ± 0.34 g OM/cm^2 for CM150; **Table 4**). While the distribution of SAP CM values is not statistically distinct from that of North America (NAM; $p > 0.64$) or Eurasia (EUR; $p > 0.56$), these findings point to an overall slightly slower recent rate of peat accumulation in the southern high-latitude regions (**Table 5**). Once the CM values were converted into RERCA 50-100-150 (g C/m^2/yr), mean values were reported at 68.31, 53.83, and 46.97 g C/m^2/yr for SAP, 113.32, 84.51, and 69.86 g C/m^2/yr for NAM, and 114.85, 91.07, and 74.78 g C/m^2/yr for EUA. To explain the difference between the SAP sites and the ones from other regions, I looked at their distribution according to the moisture and temperature bioclimatic indices, but found it is not distinct from those of other regions (**Figure 10, Figure 11**). This suggests that these climatic parameters are not the primary controls on the observed differences

in early peatland development in this region. To reiterate, it is possible that the low RERCA for SAP could be explained by our small sample size, though it is also possible that these old bogs are getting closer to their limit of peat growth (Clymo, 1984), thereby slowing down their accumulation as a result of ever-drying higher surfaces. An alternative or complementary explanation could lie in the fact that the complex topographic conditions in southern Patagonia combined with the limited number of weather stations ($n < 10$; New et al., 2002) greatly limits our capacity to adequately represent the true bioclimatic parameters of each grid cell. In particular, a climate envelope analysis (**Figure 13**) clearly indicates that SAP sites experience the mildest mean annual temperature conditions from all high-latitude peatlands, which is combined with the smallest climate seasonality (expressed as temperature of the warmest month minus temperature of the coldest month). Previous studies suggested that such unique conditions could lead to rapid accumulation; while it is true for long-term C sequestration (millennial scale), our results suggest that short-term RERCAs are not abnormally high. As a reminder, our findings do not show a difference in long-term C accumulation between SAP and other regions, though the SAP sites are near the higher-end of LORCA values for global peatlands (section 4.1).

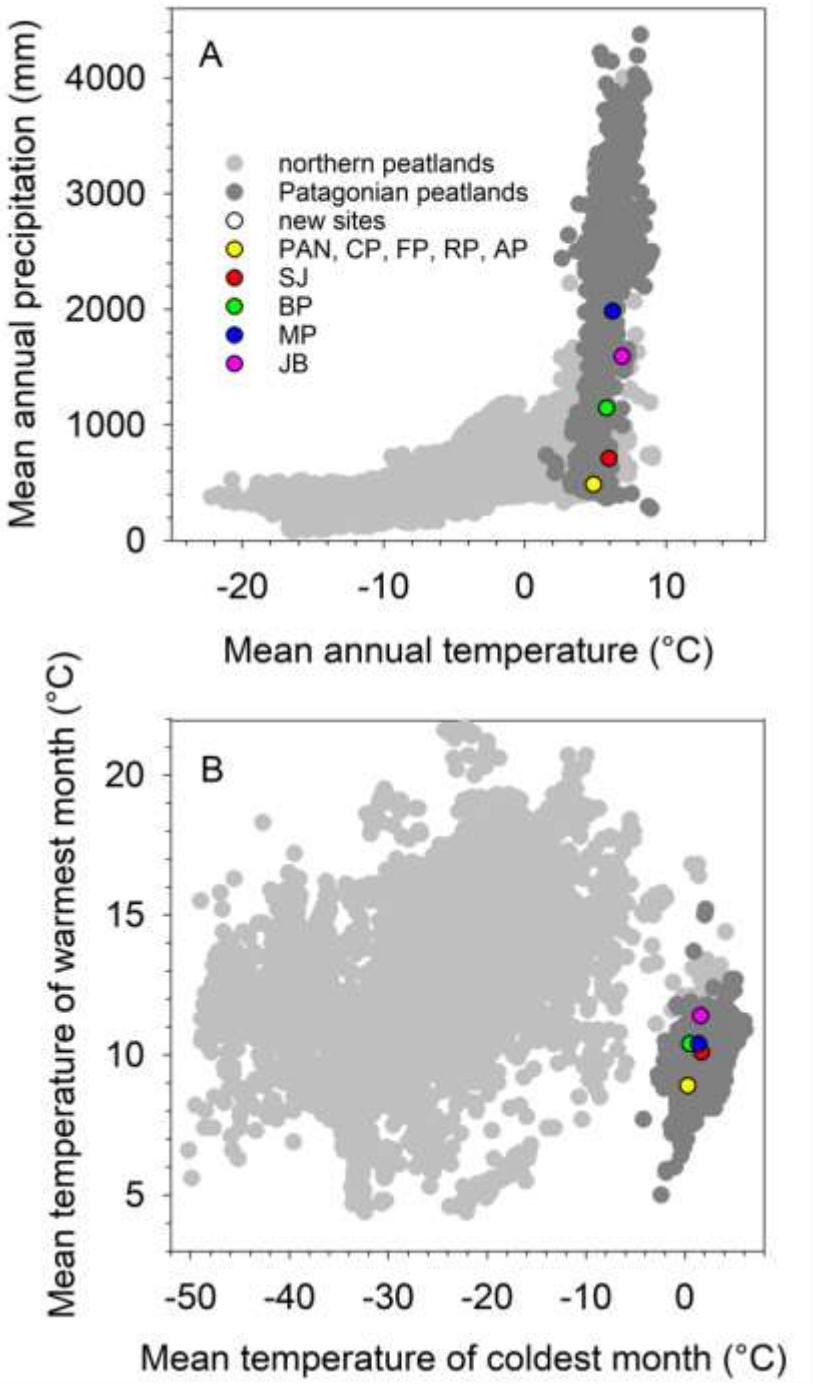

Figure 13 A climate envelope analysis. This graph highlights the differences between the Patagonian peatland climate space (dark gray circles) vs. the northern one (light gray circles). New study sites presented in this thesis (colored circles) are included. Mean annual temperature (°C) vs. total annual precipitation (mm) are presented (A), along with temperature seasonality (B). Climate data come from CRU_CL 2.0 (New et al., 2002) and are based on 1961-1990 normals; peatland area data come from Yu et al. (2010). The plots were modified from Loisel and Yu (2013b).

As expected, the Subtropics/Tropics region (STR) has the highest mean CM values (2.96 ± 2.5 g OM/cm^2 for CM50; 4.27 ± 3.7 g OM/cm^2 for CM100; 5.44 ± 5.2 g OM/cm^2 for CM150) and RERCA values (296.04 g C/m^2/yr for CM50; 213.37 g C/m^2/yr for CM100; 181.28 g C/m^2/yr for CM150), significantly greater than all three other regions (**Figure 9, Table 4**). It is likely that these sites, which are characterized by high PAR0 due to warm, year-round growing seasons, (**Figure 10**) benefit from greater C fixation potential and thus appear to accumulate large amounts of peat over short periods of time. Of course, early-diagenetic processes are not fully captured by the short-term peat mass values presented above. To test whether recent-term and long-term rates of peat accumulation are controlled by the same bioclimatic factors, I compared my short-core results (~ 100-year-old) with those from long-core results (1000-year-old) from the same sites (**Figures 10 and 11, panel D**). These millennial-scale results were first presented in Gallego-Sala et al. (2018). This comparison clearly shows the limit of PAR0 on cumulative mass over the millennial timescale, as the relationship follows a quadratic function, with low and high PAR0 both correlated with lower CM. This is a different pattern than the linear regression between PAR0 and CM that I observed for the decadal-to-centennial timescale (**Figure 10, panels A-C**). This difference between short- and long-term suggests that, while PAR0 may control short-term peat formation rates, it doesn't account much for peat decomposition, which becomes a key limit to long-term peat accumulation rates. Likewise, MI follows a decreasing negative trend as peat ages, though this is largely driven by STR data points (R^2 = -0.35; **Figure 11, panels A-C**). The latter data are characterized by high CM values and low P/E_q conditions, which seems counterintuitive. The only explanation for this trend is that STR sites receive sufficient precipitation to make peat accumulation possible, despite also losing high amounts of moisture via evapotranspiration. In fact, Gallego-Sala et al. (2018) suggest that

MI could act more like a threshold, such that a sufficient amount of moisture must be present in order for peat decay to be delayed, but increasing levels of moisture do not promote higher levels of C accumulation (**Figure 11, panel D**). Indeed, once the STR data points are removed, the correlation between CM and MI declines to -0.25 (for CM50). Lastly, it is possible that additional bioclimatic parameters are needed to better understand and constrain the relationship between CM and moisture; such indicators could include growing season P/E_q growing season moisture deficit.

5. CONCLUSIONS

5.1 Key Findings

In this study, an analysis of nine peat cores from southern Patagonia was conducted to compare their long- vs. short-term peat carbon accumulation rates. Results yielded peatland development patterns similar to those observed in other cores from the region. Nevertheless, the geochemical analysis of my new cores has provided additional paleoecological information that can be linked to the regional Holocene climate. My new cores contribute to closing local knowledge and data gaps, particularly the peatland core descriptions from a site (JB) which is, to our knowledge, the furthest north peat bog site from southern Patagonia ever studied. Another one of our sites (MP) is located in an area, due West of Puerto Natales, that does not appear to have been studied before. This core also demonstrates multiple centennial-scale fluctuations in peatland development, which point to shifts in regional atmospheric conditions that have been hinted to by previous studies. Altogether, the nine news sites also contribute new radiocarbon-based chronologies and geochemical data for future paleoclimate reconstructions and regional carbon estimates for the Karukinka Carbon Park project.

The empirical modeling approach I used to compare short-term acrotelm and the long-term catotelm carbon accumulation rates on two of the cores (BP, and MP) produced interesting results. This modeling approach allows the user to compare carbon accumulation rates from the same baseline (acrotelm/catotelm boundary), and is considered to be the most honest approach to linking long- vs. short-term carbon accumulation dynamics. While one core (MP) has potential for increased long-term carbon sequestration, the other (BP) shows a decreasing carbon-sink

capacity. This difference can be explained by local climates at each location, with the western MP site being more oceanic (it is found in a cool rain forest with cypress trees) vs. the BP site being located at the eastern boundary of the regional peat bog distribution, and embedded in the temperate beech forest. Those results are also interesting in that the BP site had, historically, been sequestering carbon at a much greater rate than site MP, and it seems as though these conditions might be switching now. It is possible that the positive shift in the AAO makes site BP too mild or dry for rapid carbon accumulation, while this slight change in climate favors site MP, which might have been too wet or cool previously. Overall, these results suggest that changing local climates could impact whether a peatland will sequester more or less carbon in the future.

A newly developed database of 186 global peatland sites detailing recent rates of carbon accumulation (past 150 years) was fitted against bioclimatic parameters that represent moisture and temperature. Results show that Patagonian peatlands are similar to other regions in terms of both their short- and long-term carbon accumulation capacities. A comparison of peat cumulative mass values at 50-100-150 years did show that the Subtropics/Tropics peat sites are the only ones that are sequestering carbon at a statistically significant greater rate ($p < 0.0001$) than any other region. This appears to be primarily due to growing seasons temperature, represented in this study as the photosynthetically active radiation for days above 0°C (PAR0). That said, this apparently high carbon sequestration potential across tropical sites over centennial timescales disappears when analyzing the same sites over millennial timescales. Indeed, the bioclimatic indices exhibited different trends for short- vs. long-term carbon sequestration. While PAR0 was linearly correlated with young peat mass, it became anti-correlated for the warmest sites, likely because over longer timescales, peat decay becomes increasingly important in controlling the

overall peat carbon mass. Although the moisture index did not exhibit a strong control on recent peat growth in most regions, it can be seen as a threshold factor for peat growth, such that a minimum amount of effective moisture is required for peatland development.

5.2 Future Research

Additional work along the nine peat cores from southern Patagonia will be required to reconstruct their developmental history. In particular, additional radiocarbon dates are needed to better constrain the chronologies and carbon sequestration rates. Likewise, detailed plant macrofossil and stable isotope analyses would provide valuable information pertaining to the millennial-scale carbon accumulation dynamics and any connection with regional climate conditions. The Karukinka cores need careful analysis of their carbon legacies to more accurately estimate the regional peat carbon stock and enable this area to become the world's first carbon conservation park.

In terms of fundamental research advancement, one way to further enhance the empirical modeling method would be to run sensitivity tests using different acrotelm decomposition times. We chose 300 years based on previous studies, but shifting this baseline upwards/downwards would allow for alternative estimates of the potential carbon transfer at the acrotelm/catotelm boundary. In addition, the database containing those 186 sites with short-term carbon dynamics should be mined to determine which sites also have "old" core data that could be used to reconstruct their entire peatland history. The empirical modeling approach could then be applied to all these sites, and a predictive picture of which regions are expected to become stronger (or weaker) carbon sinks could be drawn. This work could help land managers and policy-makers to make decisions anchored in the best possible scientific information.

The RERCA database should be expanded to include sites newly analyzed from the most recent publications (I stopped mining data in August 2019), as well as those being currently analyzed from new data collection. Ideally, this database would be utilized as a hub for storing peatland carbon accumulation data; it will be made publicly available on the PANGAEA platform. This easy data access will enable researchers to use my work to better predict the carbon storage capacity of global peatlands for the future and compare it with past carbon-sink capacity. The development of additional bioclimatic indices (section 4.3) could provide a new and more comprehensive understanding of peatland response to different aspects of environmental change. Finally, this database could provide the basis for a new generation of studies focusing on recent peatland carbon dynamics, which is needed to help guide management, including land conversion, policy, and restoration.

REFERENCES

ADKINSON, A. C., SYED, K. H. & FLANAGAN, L. B. 2011. Contrasting responses of growing season ecosystem CO2 exchange to variation in temperature and water table depth in two peatlands in northern Alberta, Canada. *Journal of Geophysical Research: Biogeosciences,* 116.

AUER, V. 1958. The Pleistocene of Fuego-Patagonia, Part II. The history of the flora and vegetation. *Ann. Acad. Sci. Fenn. Ser. III,* 50: 1-239

BELYEA, L. R. & MALMER, N. 2004. Carbon sequestration in peatland: patterns and mechanisms of response to climate change. *Global Change Biology,* 10**,** 1043-1052.

BENTLEY, M. J. & MCCULLOCH, R. 2005. Impact of neotectonics on the record of glacier and sea level fluctuations, Strait of Magellan, southern Chile. *Geografiska Annaler: Series A, Physical Geography,* 87**,** 393-402.

BLAAUW, M. & CHRISTEN, J. A. 2011. Flexible paleoclimate age-depth models using an autoregressive gamma process. *Bayesian Analysis,* 6**,** 457-474.

BLODAU, C. & MOORE, T. R. 2002. Macroporosity affects water movement and pore water sampling in peat soils. *Soil Science,* 167**,** 98-109.

CAI, T., FLANAGAN, L. B. & SYED, K. H. 2010. Warmer and drier conditions stimulate respiration more than photosynthesis in a boreal peatland ecosystem: analysis of automatic chambers and eddy covariance measurements. *Plant, Cell & Environment,* 33**,** 394-407.

CAI, W., WHETTON, P. H. & KAROLY, D. J. 2003. The response of the Antarctic Oscillation to increasing and stabilized atmospheric CO2. *Journal of Climate,* 16**,** 1525-1538.

CHARMAN, D. J., BEILMAN, D. W., JACKSON, S., KORHOLA, A., MAUQUOY, D., MITCHELL, F., PRENTICE, I., VAN DER LINDEN, M., DE VLEESCHOUWER, F. & YU, Z. 2013. Climate-related changes in peatland carbon accumulation during the last millennium. *Biogeosciences,* 1-, 924-944.

Climate-Data.org 2020. *XII Region of Magallanes and Chilean Antarctica Climate,* viewed 1st October, 2019, <https://en.climate-data.org/south-america/chile/xii-region-of-magallanes-and-chilean-antarctica-74/>

CLYMO, R. 1965. Experiments on breakdown of Sphagnum in two bogs. *The Journal of Ecology***,** 747-758.

CLYMO, R. 1984. The limits to peat bog growth. *Phil. Trans. R. Soc. Lond. B,* 303**,** 605-654.

DEAN, W. E. 1974. Determination of carbonate and organic matter in calcareous sediments and sedimentary rocks by loss on ignition; comparison with other methods. *Journal of Sedimentary Research,* 44**,** 242-248.

DORREPAAL, E., TOET, S., VAN LOGTESTIJN, R. S., SWART, E., VAN DE WEG, M. J., CALLAGHAN, T. V. & AERTS, R. 2009. Carbon respiration from subsurface peat accelerated by climate warming in the subarctic. *Nature,* 460**,** 616-619.

FRIEDLINGSTEIN, P., COX, P., BETTS, R., BOPP, L., VON BLOH, W., BROVKIN, V., CADULE, P., DONEY, S., EBY, M. & FUNG, I. 2006. Climate–carbon cycle feedback analysis: results from the C4MIP model intercomparison. *Journal of Climate,* 19**,** 3337-3353.

FROLKING, S., ROULET, N. T., MOORE, T. R., RICHARD, P. J., LAVOIE, M. & MULLER, S. D. 2001. Modeling northern peatland decomposition and peat accumulation. *Ecosystems,* 4**,** 479-498.

FROLKING, S., TALBOT, J., JONES, M. C., TREAT, C. C., KAUFFMAN, J. B., TUITTILA, E.-S. & ROULET, N. 2011. Peatlands in the Earth's 21st century climate system. *Environmental Reviews,* 19**,** 371-396.

GALLEGO-SALA, A. V., CHARMAN, D. J., BREWER, S., PAGE, S. E., PRENTICE, I. C., FRIEDLINGSTEIN, P., MORETON, S., AMESBURY, M. J., BEILMAN, D. W. & BJÖRCK, S. 2018. Latitudinal limits to the predicted increase of the peatland carbon sink with warming. *Nature Climate Change,* 8**,** 907.

GARREAUD, R. 2009. The Andes climate and weather. *Advances in Geosciences,* 22**,** 3.

GILLETT, N. P., KELL, T. D. & JONES, P. 2006. Regional climate impacts of the Southern Annular Mode. *Geophysical Research Letters,* 33.

GORHAM, E. 1991. Northern peatlands: role in the carbon cycle and probable responses to climatic warming. *Ecological Applications,* 1**,** 182-195.

GRAVERSEN, R. G., MAURITSEN, T., TJERNSTRÖM, M., KÄLLÉN, E. & SVENSSON, G. 2008. Vertical structure of recent Arctic warming. *Nature,* 451**,** 53-56.

GROOTJANS, A., ITURARRASPE, R., LANTING, L., FRITZ, C. & JOOSTEN, H. 2010. Ecohydrological features of some contrasting mires of tierra del fuego, argentina. *Mires and Peat*, 6, 1-15.

HANSEN, J., SATO, M., RUEDY, R., LO, K., LEA, D. W. & MEDINA-ELIZADE, M. 2006. Global temperature change. *Proceedings of the National Academy of Sciences,* 103**,** 14288-14293.

HOGG, A., TURNEY, C., PALMER, J., COOK, E. & BUCKLEY, B. 2013. Is there any Evidence for Regional Atmospheric 14 C Offsets in the Southern Hemisphere? *Radiocarbon,* 55**,** 2029-2034.

HUA, Q. & BARBETTI, M. 2004. Review of tropospheric bomb 14 C data for carbon cycle modeling and age calibration purposes. *Radiocarbon,* 46**,** 1273-1298.

HUBER, U. M. & MARKGRAF, V. 2003. Holocene fire frequency and climate change at Rio Rubens Bog, southern Patagonia. *Fire and Climatic Change in Temperate Ecosystems of the Western Americas.* Springer.

ISE, T., DUNN, A. L., WOFSY, S. C. & MOORCROFT, P. R. 2008. High sensitivity of peat decomposition to climate change through water-table feedback. *Nature Geoscience,* 1**,** 763-766.

KAPLAN, M., SCHAEFER, J., STRELIN, J. A., DENTON, G., ANDERSON, R., VANDERGOES, M., FINKEL, R., SCHWARTZ, R., TRAVIS, S. & GARCIA, J. 2016. Patagonian and southern South Atlantic view of Holocene climate. *Quaternary Science Reviews,* 141**,** 112-125.

KELLER, J. K. & BRIDGHAM, S. D. 2007. Pathways of anaerobic carbon cycling across an ombrotrophic-minerotrophic peatland gradient. *Limnology and Oceanography,* 52**,** 96-107.

KELLER, J. K., WHITE, J. R., BRIDGHAM, S. D. & PASTOR, J. 2004. Climate change effects on carbon and nitrogen mineralization in peatlands through changes in soil quality. *Global Change Biology,* 10, 1053-1064.

KILIAN, R., BIESTER, H., BEHRMANN, J., BAEZA, O., FESQ-MARTIN, M., HOHNER, M., SCHIMPF, D., FRIEDMANN, A. & MANGINI, A. 2006. Millennium-scale volcanic impact on a superhumid and pristine ecosystem. *Geology,* 34**,** 609-612.

KILIAN, R., HOHNER, M., BIESTER, H., WALLRABE-ADAMS, H. J. & STERN, C. R. 2003. Holocene peat and lake sediment tephra record from the southernmost Chilean Andes (53-55 S). *Revista Geologica de Chile,* 30**,** 23-37.

LAMY, F., KILIAN, R., ARZ, H. W., FRANCOIS, J.-P., KAISER, J., PRANGE, M. & STEINKE, T. 2010. Holocene changes in the position and intensity of the southern westerly wind belt. *Nature Geoscience,* 3**,** 695-699.

LEIFELD, J., WÜST-GALLEY, C. & PAGE, S. 2019. Intact and managed peatland soils as a source and sink of GHGs from 1850 to 2100. *Nature Climate Change,* 9**,** 945-947.

LOISEL, J., GALLEGO-SALA, A. V. & YU, Z. 2012. Global-scale pattern of peatland Sphagnum growth driven by photosynthetically active radiation and growing season length. *Biogeosciences,* 9, 2737-2746.

LOISEL, J. & YU, Z. 2013a. Recent acceleration of carbon accumulation in a boreal peatland, south central Alaska. *Journal of Geophysical Research: Biogeosciences,* 118**,** 41-53.

LOISEL, J. & YU, Z. 2013b. Holocene peatland carbon dynamics in Patagonia. *Quaternary Science Reviews,* 69**,** 125-141.

LOISEL, J. & YU, Z. 2013c. Surface vegetation patterning controls carbon accumulation in peatlands. *Geophysical Research Letters,* 40**,** 5508-5513.

LOISEL, J., YU, Z., BEILMAN, D. W., CAMILL, P., ALM, J., AMESBURY, M. J., ANDERSON, D., ANDERSSON, S., BOCHICCHIO, C. & BARBER, K. 2014. A database and synthesis of northern peatland soil properties and Holocene carbon and nitrogen accumulation. *The Holocene,* 24**,** 1028-1042.

LOISEL, J. 2015. Peatlands as carbon sinks / Las turberas como sumideros de carbono, Chapter 11 p. 297-315. In: E Domínguez and D Vega-Valdés (eds.). *Funciones y Servicios Ecosistémicos de las Turberas en Magallanes.* INIA Nº 33. Punta Arenas, Chile. 334 pp.

LOURENÇATO, L. F., CALDEIRA, P. P., BERNARDES, M. C., BUCH, A. C., TEIXEIRA, D. C. & SILVA-FILHO, E. V. 2017. Carbon accumulation rates recorded in the last 150 years in tropical high mountain peatlands of the Atlantic Rainforest, SE-Brazil. *Science of the Total Environment,* 579**,** 439-446.

MANABE, S. & STOUFFER, R. J. 1980. Sensitivity of a global climate model to an increase of CO2 concentration in the atmosphere. *Journal of Geophysical Research: Oceans,* 85**,** 5529-5554.

MANSILLA, C., MCCULLOCH, R. D., MORELLO, F. 2016. *Extending the tephrochronology of Fuego-Patagonia, southern South America (~53°S).* [Poster]. VII Southern Connections at Punta Arenas, Chile. January, 2016

MCCULLOCH, R. D. & DAVIES, S. J. 2001. Late-glacial and Holocene palaeoenvironmental change in the central Strait of Magellan, southern Patagonia. *Palaeogeography, Palaeoclimatology, Palaeoecology,* 173**,** 143-173.

MCCULLOCH, R. D., MANSILLA, C. A., MORELLO, F., DE POL-HOLZ, R., SAN ROMAN, M., TISDALL, E. & TORRES, J. 2019. Late glacial and Holocene landscape change and rapid climate and coastal impacts in the Canal Beagle, southernmost Patagonia. *Journal of Quaternary Science*, 34(8), 674-684.

MCGUIRE, A. D., ANDERSON, L. G., CHRISTENSEN, T. R., DALLIMORE, S., GUO, L., HAYES, D. J., HEIMANN, M., LORENSON, T. D., MACDONALD, R. W. & ROULET, N. 2009. Sensitivity of the carbon cycle in the Arctic to climate change. Ecological Monographs, 79, 523-555.

MOORE, D. M. 1983. Flora of Tierra del Fuego. *Flora of Tierra del Fuego.*

MORENO, P., FRANÇOIS, J. P., VILLA-MARTÍNEZ, R. & MOY, C. 2009. Millennial-scale variability in Southern Hemisphere westerly wind activity over the last 5000 years in SW Patagonia. *Quaternary Science Reviews,* 28**,** 25-38.

MORENO, P., VILANOVA, I., VILLA-MARTÍNEZ, R., DUNBAR, R., MUCCIARONE, D., KAPLAN, M., GARREAUD, R., ROJAS, M., MOY, C. & DE POL-HOLZ, R. 2018. Onset and evolution of southern annular mode-like changes at centennial timescale. *Scientific Reports,* 8**,** 1-9.

MORENO, P. I., FRANCOIS, J.-P., MOY, C. & VILLA-MARTÍNEZ, R. 2010. Covariability of the Southern Westerlies and atmospheric CO2 during the Holocene. *Geology,* 38**,** 727-730.

MORENO, P. I., VILANOVA, I., VILLA-MARTÍNEZ, R., GARREAUD, R., ROJAS, M. & DE POL-HOLZ, R. 2014. Southern Annular Mode-like changes in southwestern Patagonia at centennial timescales over the last three millennia. *Nature Communications,* 5**,** 1-7.

MYERS-SMITH, I. H., FORBES, B. C., WILMKING, M., HALLINGER, M., LANTZ, T., BLOK, D., TAPE, K. D., MACIAS-FAURIA, M., SASS-KLAASSEN, U. & LÉVESQUE, E. 2011. Shrub expansion in tundra ecosystems: dynamics, impacts and research priorities. *Environmental Research Letters,* 6**,** 045509.

NEW, M., LISTER, D., HULME, M. & MAKIN, I. 2002. A high-resolution data set of surface climate over global land areas. *Climate Research,* 21**,** 1-25.

PACKALEN, M. S. & FINKELSTEIN, S. A. 2014. Quantifying Holocene variability in carbon uptake and release since peat initiation in the Hudson Bay Lowlands, Canada. *The Holocene,* 24**,** 1063-1074.

PARUELO, J. M., BELTRÁN, A., JOBBÁGY, E., SALA, O. E. & GOLLUSCIO, R. A. 1998. The climate of Patagonia: general patterns and controls on biotic processes. *Ecología Austral,* 8**,** 085-101.

PERI, P. L., ROSAS, Y. M., LADD, B., TOLEDO, S., LASAGNO, R. G. & MARTÍNEZ PASTUR, G. 2018. Modelling soil carbon content in South Patagonia and evaluating changes according to climate, vegetation, desertification and grazing. *Sustainability,* 10**,** 438.

PISANO, E. 1983. Magellanic Tundra complex. *Ecosystems of the World*.

PRENTICE, I. C., SYKES, M. T. & CRAMER, W. 1993. A simulation model for the transient effects of climate change on forest landscapes. *Ecological Modelling,* 65**,** 51-70.

RABASSA, J., CORONATO, A., HEUSSER, C., JUÑENT, F. R., BORROMEI, A., ROIG, C. & QUATTROCCHIO, M. 2006. The peatlands of Argentine Tierra del Fuego as a source for paleoclimatic and paleoenvironmental information. *Developments in Earth Surface Processes,* 9**,** 129-144.

RASTETTER, E. B., RYAN, M. G., SHAVER, G. R., MELILLO, J. M., NADELHOFFER, K. J., HOBBIE, J. E. & ABER, J. D. 1991. A general biogeochemical model describing the responses of the C and N cycles in terrestrial ecosystems to changes in CO2, climate, and N deposition. *Tree Physiology,* 9**,** 101-126.

REIMER, P. J., BARD, E., BAYLISS, A., BECK, J. W., BLACKWELL, P. G., RAMSEY, C. B., BUCK, C. E., CHENG, H., EDWARDS, R. L. & FRIEDRICH, M. 2013. IntCal13 and Marine13 radiocarbon age calibration curves 0–50,000 years cal BP. *Radiocarbon,* 55**,** 1869-1887.

REIMER, P. J., BROWN, T. A. & REIMER, R. W. 2004. Discussion: reporting and calibration of post-bomb 14C data. *Radiocarbon,* 46**,** 1299-1304.

ROIG JR, F., ROIG, C., RABASSA, J. & BONINSEGNA, J. 1996. Fuegian floating tree-ring chronology from subfossil Nothofagus wood. *The Holocene,* 6**,** 469-476.

RYDIN, H. & JEGLUM, J. 2006. Peatlands around the world. Oxford University Press: Oxford.

SHENG, Y., SMITH, L. C., MACDONALD, G. M., KREMENETSKI, K. V., FREY, K. E., VELICHKO, A. A., LEE, M., BEILMAN, D. W. & DUBININ, P. 2004. A high-resolution GIS-based inventory of the west Siberian peat carbon pool. *Global Biogeochemical Cycles,* 18.

STERN, C. R. 2008. Holocene tephrochronology record of large explosive eruptions in the southernmost Patagonian Andes. *Bulletin of Volcanology,* 70**,** 435-454.

STRELIN, J., DENTON, G., VANDERGOES, M., NINNEMANN, U. & PUTNAM, A. 2011. Radiocarbon chronology of the late-glacial Puerto Bandera moraines, southern Patagonian Icefield, Argentina. *Quaternary Science Reviews,* 30**,** 2551-2569.

STRELIN, J. A., KAPLAN, M. R., VANDERGOES, M. J., DENTON, G. H. & SCHAEFER, J. M. 2014. Holocene glacier history of the Lago Argentino basin, southern Patagonian Icefield. *Quaternary Science Reviews,* 101**,** 124-145.

SWANN, A. L., FUNG, I. Y., LEVIS, S., BONAN, G. B. & DONEY, S. C. 2010. Changes in Arctic vegetation amplify high-latitude warming through the greenhouse effect. *Proceedings of the National Academy of Sciences,* 107**,** 1295-1300.

TURETSKY, M. R., BENSCOTER, B., PAGE, S., REIN, G., VAN DER WERF, G. R. & WATTS, A. 2015. Global vulnerability of peatlands to fire and carbon loss. *Nature Geoscience,* 8, 11.

TURUNEN, J., TOMPPO, E., TOLONEN, K. & REINIKAINEN, A. 2002. Estimating carbon accumulation rates of undrained mires in Finland–application to boreal and subarctic regions. *The Holocene,* 12**,** 69-80.

UPDEGRAFF, K., BRIDGHAM, S. D., PASTOR, J., WEISHAMPEL, P. & HARTH, C. 2001. Response of CO2 and CH4 emissions from peatlands to warming and water table manipulation. *Ecological Applications,* 11**,** 311-326.

VAN BELLEN, S., MAUQUOY, D., HUGHES, P. D., ROLAND, T. P., DALEY, T. J., LOADER, N. J., STREET-PERROTT, F. A., RICE, E. M., PANCOTTO, V. A. & PAYNE, R. J. 2016. Late-Holocene climate dynamics recorded in the peat bogs of Tierra del Fuego, South America. *The Holocene,* 26**,** 489-501.

VOGEL, J. S., SOUTHON, J. R. & NELSON, D. E. 1987. Catalyst and binder effects in the use of filamentous graphite for AMS. *Nuclear Instruments and Methods in Physics Research Section B: Beam Interactions with Materials and Atoms,* 29**,** 50-56.

WEIDEMANN, S. S., SAUTER, T., KILIAN, R., STEGER, D., BUTOROVIC, N. & SCHNEIDER, C. 2018. A 17-year record of meteorological observations across the gran campo nevado ice cap in southern patagonia, Chile, related to synoptic weather types and climate modes. *Frontiers in Earth Science,* 6**,** 53.

XIA, Z., YU, Z. & LOISEL, J. 2018. Centennial-scale dynamics of the Southern Hemisphere Westerly Winds across the Drake Passage over the past two millennia. *Geology,* 46**,** 855-858.

YOUNG, D. M., BAIRD, A. J., CHARMAN, D. J., EVANS, C. D., GALLEGO-SALA, A. V., GILL, P. J., HUGHES, P. D., MORRIS, P. J. & SWINDLES, G. T. 2019. Misinterpreting carbon accumulation rates in records from near-surface peat. *Scientific Reports,* 9**,** 1-8.

YU, Z. 2011. Holocene carbon flux histories of the world's peatlands: Global carbon-cycle implications. *The Holocene,* 21**,** 761-774.

YU, Z. 2012. Northern peatland carbon stocks and dynamics: a review. *Biogeosciences,* 9**,** 4071-4085.

YU, Z., BEILMAN, D. W. & JONES, M. C. 2009. Sensitivity of northern peatland carbon dynamics to Holocene climate change. *Carbon Cycling in Northern Peatlands,* 184**,** 55-69.

YU, Z., LOISEL, J., BROSSEAU, D. P., BEILMAN, D. W. & HUNT, S. J. 2010. Global peatland dynamics since the Last Glacial Maximum. *Geophysical Research Letters,* 37.

APPENDIX A

SUPPLEMENTARY TABLES

Supplementary Table A1 Global database of recent rates of carbon accumulation (RERCA), site contributor and location information.

Reference	*Contributor*	*Site Code*	*long.*	*lat.*	*Region (EUA, NAM, STR, SAP)*
unpublished	Blyakharchuk	Nadym	87.8333	55.8833	EUA
unpublished	Blyakharchuk	Shestakovo	72.8742	65.3155	EUA
De Vleeshouwer et al. (2009)	De Vleeschouwer	Słowińskie Błota	16.49	54.36	EUA
De Vleeshouwer et al. (2012)	DeVleeschouwer	Misten_Bog	6.1642	50.5631	EUA
unpublished	Diaconu	Molhasul	22.76	46.59	EUA
Feurdean et al. (2015)	Feurdean	Taul Muced	24.32	47.34	EUA
Fialkiewicz-Koziel et al. (2014)	Fialkiawicz-Koziel	Bagno_Mikoleska	18.8172	50.5606	EUA
Fialkiewicz-Koziel et al. (2014)	Fialkiawicz-Koziel	Pusczina_Mala	19.0867	49.0544	EUA
Fialkiewicz-Koziel et al. (2014)	Fialkiewicz-Koziel	PK	19.56	49.28	EUA
Givelet et al. (2004)	Givelet	Étang de la Gruyère 2f	7.03	47.23	EUA
Givelet et al. (2004)	Givelet	Étang de la Gruyère 2k	7.03	47.23	EUA
Heinemeyer and Swindles (2018)	Heinemeyer	Moor House	-2.37	54.68	EUA
Heinemeyer et al. (2018)	Heinemeyer	Mossdale	-2.17	54.19	EUA
Heinemeyer et al. (2018)	Heinemeyer	Nidderdale	-1.55	54.1	EUA
Heinemeyer et al. (2018)	Heinemeyer	Whitendale	-2.3	53.59	EUA
Hendon and Charman (2004)	Hendon	BFA	-2.5	55.08	EUA
Hendon and Charman (2004)	Hendon	BFB	-2.5	55.08	EUA
unpublished	Karofeld	Mannikjarvi	26.2556	58.8753	EUA
Kokfelt et al. (2010)	Kokfelt	Stordalen_Kokfelt	19.05	68.35	EUA
Marcisz et al. (2015)	Lamentowicz	Linje_Mire	18.3111	53.1889	EUA
Enrico et al. (2017)	LeRoux	ESTIBERE	0.17	42.83	EUA

unpublished	LeRoux	Kolhütten	8.18	47.93	EUA
Enrico et al. (2017)	LeRoux	Pinet A	1.97	42.85	EUA
Enrico et al. (2017)	LeRoux	Pinet B	1.97	42.85	EUA
Enrico et al. (2017)	LeRoux	Pinet C	1.97	42.85	EUA
Liu et al. (2019)	Liu	Honghe	133.63	47.79	EUA
Liu et al. (2019)	Liu	Hongtu	124.24	51.62	EUA
Liu et al. (2019)	Liu	Huyuan	123.63	51.94	EUA
Liu et al. (2019)	Liu	Shenjiadian	130.66	46.58	EUA
Liu et al. (2019)	Liu	Tuquiang	122.85	52.94	EUA
unpublished	Makila	Hanhijanka	27.15	69.1667	EUA
Mäkilä and Moisanen (2007)	Makila	Luovuoma	23.4333	68.4	EUA
Lamentowicz et al. (acc.)	Marcisz	Głęboczek	18.21	53.88	EUA
Marcisz et al. (2015)	Marcisz	Linje	18.31	53.19	EUA
Charman et al. (2013)	Mitchell	Balyduff	-6.0069	53.0861	EUA
Novak et al. (2007)	Novak	Connemara	-10	53.24	EUA
Novak et al. (2007)	Novak	Mull	-6.17	56.18	EUA
Novak et al. (2007)	Novak	Ocean Bog	13.3	49.03	EUA
Novak et al. (2007)	Novak	Rybarenska slat	13.3	49.03	EUA
Novak et al. (2007)	Novak	Thorne Moors	-0.52	53.24	EUA
Oldfield et al. (1994)	Oldfield	BM	-4.73	55.38	EUA
Oldfield et al. (1994)	Oldfield	EM	-4.3798713	55.086647	EUA
Oldfield et al. (1994)	Oldfield	HW	-3.06	54.31	EUA
Oldfield et al. (1994)	Oldfield	RM	-1.53	53.46	EUA
Olid et al. (2014)	Olid	Degerö Stormyr	19.33	64.11	EUA
Olid et al. (2016)	Olid	CHL-13	-7.5	43.5	EUA
Olid et al. (2016)	Olid	SM-1	13.92	57.25	EUA
Olid et al. (2016)	Olid	SM-2	13.92	57.25	EUA
Olid et al. (2016)	Olid	SM-3	13.92	57.25	EUA
Orme et al. (2017)	Orme	Pedrido	-7.5292	43.4503	EUA
Parry et al. (2013)	Parry	Control, 6	3.999	50.601	EUA
Parry et al. (2013)	Parry	Control, 7	3.999	50.601	EUA

Parry et al. (2013)	Parry	Control, 8	3.999	50.601	EUA
Sanchez-Cabeza et al. (2014)	Sanchez-Cabeza	SEMARNAT	-7.56	43.5	EUA
Shotyk et al. (2005)	Shotyk	Myranar 2	-7.17	62.15	EUA
Swindles et al. (2015)	Swindles	Craterpool_1	19.8576	68.3195	EUA
Swindles et al. (2015)	Swindles	Craterpool_2	19.8576	68.3195	EUA
Swindles et al. (2010)	Swindles	Dead_Island	-6.5491	54.8875	EUA
Swindles et al. (2015)	Swindles	Eagle_Bog	19.5841	68.3657	EUA
Swindles et al. (2015)	Swindles	Electric_Bog	19.3684	67.8656	EUA
Swindles et al. (2015)	Swindles	Instrument_Bog	19.7656	68.1979	EUA
Swindles et al. (2015)	Swindles	Marooned	19.9865	67.9567	EUA
Swindles et al. (2015)	Swindles	Nikka	19.1785	67.8673	EUA
Swindles et al. (2015)	Swindles	Railway_Bog	19.8314	68.0868	EUA
Swindles et al. (2015)	Swindles	Stordalen_Internal	19.0442	68.3564	EUA
Swindles et al. (2015)	Swindles	Stordalen_Swindles	19.0442	68.3564	EUA
Turner et al. (2016)	Turner	Malham_Tarn	-2.175	54.0964	EUA
Ukonmaanaho et al. (2006)	Ukonmaanaho	Harjavalta	22.11	61.21	EUA
Ukonmaanaho et al. (2006)	Ukonmaanaho	Hietajarvi	30.4	63.09	EUA
Ukonmaanaho et al. (2006)	Ukonmaanaho	Outokumpu	28.51	62.4	EUA
Zhang et al. (2018)	Zhang	Ind1	49.53	67.16	EUA
Zhang et al. (2018)	Zhang	Ind2	49.53	67.16	EUA
Zhang et al. (2018)	Zhang	Ind4	49.88	67.27	EUA
Zhang et al. (2018)	Zhang	Ind5	49.88	67.27	EUA
Zhang et al. (2018)	Zhang	Kev2	27.17	69.82	EUA
Zhang et al. (2018)	Zhang	Kil	21.3	68.53	EUA
Zhang et al. (2018)	Zhang	Kil2	21.05	68.88	EUA
Zhang et al. (2019; manu.)	Zhang	LHL	24.32	61.8	EUA
Zhang et al. (2019; manu.)	Zhang	LLH	24.32	61.8	EUA
Zhang et al. (2019; manu.)	Zhang	LLL	24.32	61.8	EUA
Zhang et al. (2019; manu.)	Zhang	SHL	24.17	61.83	EUA
Zhang et al. (2019; manu.)	Zhang	SLH	24.17	61.83	EUA
Zhang et al. (2019; manu.)	Zhang	SLL	24.17	61.83	EUA
Ali et al. (2008)	Ali	Aéroport 1	-72.5	53.83	NAM

Ali et al. (2008)	Ali	Aéroport 4	-72.5	53.83	NAM
Ali et al. (2008)	Ali	Aéroport 5	-72.5	53.83	NAM
Ali et al. (2008)	Ali	Ours 1	-72.46	54.06	NAM
Ali et al. (2008)	Ali	Ours 4	-72.46	54.06	NAM
Bauer et al. (2009)	Bauer	Old Black Spruce 3	-105.12	54	NAM
Bauer et al. (2009)	Bauer	Sandhill Fen 4	-104.63	53.83	NAM
Belyea and Warner (1996)	Belyea	DaS	-94.55	48.78	NAM
Belyea and Warner (1996)	Belyea	DcC	-94.55	48.78	NAM
Belyea and Warner (1996)	Belyea	HfC	-94.55	48.78	NAM
Belyea and Warner (1996)	Belyea	HfS	-94.55	48.78	NAM
unpublished	Booth	Sidnaw	-88.78	46.56	NAM
Bunbury et al. (2012)	Bunbury	VC04-6	-84.18	52.71	NAM
Charman et al. (2015)	Charman	Petite_Bog	-63.9392	45.1514	NAM
unpublished	Clifford	Burns_Bog	-122.9647	49.1145	NAM
unpublished	Clifford	Surrey_Bog	-122.746	49.205	NAM
Davies et al. (2018)	Davies	ANZ	-111.0497	56.4854	NAM
Davies et al. (2018)	Davies	JPH	-111.414	57.1029	NAM
Davies et al. (2018)	Davies	McK	-111.7161	57.191	NAM
Davies et al. (2018)	Davies	McM	-111.2458	56.6321	NAM
Davies et al. (2018)	Davies	MIL	-111.4677	56.9115	NAM
Davies et al. (2018)	Davies	UTK*	-113.86	55.97	NAM
Van Bellen et al. (2013)	Garneau	AERO_1	-72.52	54.1	NAM
Magnan and Garneau (2014)	Garneau	BAIE_2_Garneau	-68.2333	49.0667	NAM
Pratte et al. (2013)	Garneau	Mer_Bleue_Garneau	-75.8	45.6833	NAM
Hughes et al. (2006)	Hugues	Nordan	-53.58	49.15	NAM
unpublished	Klein	Fish_Creek	-134.555	58.336	NAM
unpublished	Klein	Point_lena	-134.746	58.386	NAM
Lamarre et al. (2012)	Lamarre	KUJU_PD2	-77.7	55.23	NAM
Lavoie et al. (2013)	Lavoie	Covey_Hill	-73.49	45	NAM
Loisel and Garneau (2010)	Loisel	Lac Le Caron RiP2	-75.83	52.28	NAM
Loisel and Garneau (2010)	Loisel	Mosaik RiP2	-75.4	51.97	NAM

McFarlane et al. (2018)	McFarlane	8T	-93.27	47.31	NAM
Piilo et al. (2019)	Piilo	K1P1	-77.69	55.23	NAM
Piilo et al. (2019)	Piilo	K1P2	-77.69	55.23	NAM
Piilo et al. (2019)	Piilo	K1P3	-77.69	55.23	NAM
Piilo et al. (2019)	Piilo	K2.1	-77.71	55.23	NAM
Piilo et al. (2019)	Piilo	K2.2	-77.71	55.23	NAM
Piilo et al. (2019)	Piilo	LG2.1	-77.73	53.65	NAM
Piilo et al. (2019)	Piilo	LG2.3	-77.73	53.65	NAM
Piilo et al. (2019)	Piilo	Rad1	-77.75	53.66	NAM
Piilo et al. (2019)	Piilo	Rad2	-77.75	53.66	NAM
Piilo et al. (2019)	Piilo	Rad3	-77.75	53.66	NAM
Sanderson (2016)	Sanderson	BAIE_2_Sanderson	-68.15	49.06	NAM
Sanderson (2016)	Sanderson	Lebel	-68.14	49.07	NAM
Sanderson (2016)	Sanderson	Morts	-63.4	50.16	NAM
Sanderson (2016)	Sanderson	Plaine	-63.32	50.16	NAM
Sanderson (2016)	Sanderson	Red_Bay	-56.25	51.46	NAM
Sanderson (2016)	Sanderson	Romaine	-63.41	50.17	NAM
Sanderson (2016)	Sanderson	Vallee	-57.11	51.29	NAM
Shotyk et al. (2003)	Shotyk	Tasiusaq	-45.5617	61.1386	NAM
Sim et al. (2019)	Sim	Coastal Fen A	-105.46	68.65	NAM
Sim et al. (2019)	Sim	Coastal Fen B	-105.46	68.65	NAM
Taylor et al. (2019)	Taylor	TFS1	-149.6	68.62	NAM
Taylor et al. (2019)	Taylor	TFS2	-149.6	68.62	NAM
Turetsky et al. (2007)	Turetsky	Anzac 1	-111.22	56.65	NAM
Turetsky et al. (2007)	Turetsky	Anzac 2	-111.22	56.65	NAM
Turetsky et al. (2007)	Turetsky	Moose Lake	-101.1	53.97	NAM
Turetsky et al. (2007)	Turetsky	Patuanak	-108.52	54.12	NAM
Vitt et al. (2009)	Vitt	Edson	-116.75	53.58	NAM
Vitt et al. (2009)	Vitt	Hondo	-114.12	55.12	NAM
Vitt et al. (2009)	Vitt	Saulteaux	-114.17	55.12	NAM
Wieder et al. (1994)	Wieder	Big Run	-79.55	39.12	NAM
Wieder et al. (1994)	Wieder	Cranesville	-79.52	39.43	NAM

Wieder et al. (1994)	Wieder	Marcell	-93.47	47.53	NAM
Wieder et al. (1994)	Wieder	Tamarack	-75.63	41.25	NAM
Wieder et al. (1994)	Wieder	Tub Run	-79.55	39.12	NAM
unpublished	Bunsen	BP	-71.935	-52.057	SAP
unpublished	Bunsen	MP	-72.849	-51.752	SAP
León and Oliván (2014)	Leon	CA	-74	-42.5	SAP
León and Oliván (2014)	Leon	CH	-74	-42.5	SAP
León and Oliván (2014)	Leon	PL	-74	-42.5	SAP
León and Oliván (2014)	Leon	SD	-74	-42.5	SAP
León and Oliván (2014)	Leon	TG	-74	-42.5	SAP
Van Bellen et al. (2016)	Roland	Karukinka_A_B	-69.5764	-53.86	SAP
Van Bellen et al. (2016)	Roland	Pulpito	-73.7814	-42.7583	SAP
Van Bellen et al. (2016)	Roland	Tierra_Australis	-67.7707	-54.6162	SAP
unpublished	Charman; Gallego-Sala	Sebangau_1A	113.9039	-2.3231	STR
unpublished	Charman; Gallego-Sala	Sebangau_1B	113.9034	-2.3224	STR
unpublished	Charman; Gallego-Sala	Sebangau_2A	113.8968	-2.3312	STR
unpublished	Charman; Gallego-Sala	Sebangau_2B	113.8966	-2.3311	STR
unpublished	Charman; Gallego-Sala	Sebangau_3A	113.8908	-2.3377	STR
unpublished	Charman; Gallego-Sala	Sebangau_3B	113.8903	-2.3375	STR
unpublished	Charman; Gallego-Sala	Sebangau_4A	113.8866	-2.3159	STR
unpublished	Charman; Gallego-Sala	Sebangau_5A	113.8838	-2.3209	STR
unpublished	Charman; Gallego-Sala	Sebangau_5B	113.8838	-2.3214	STR
Li et al. (2017)	Li	Amsterdam Island	77.33	-37.51	STR
Lourençato et al. (2017)	Lourençato	INP	-44.37	-22.18	STR
Lourençato et al. (2017)	Lourençato	SONP	-43.2	-22.28	STR
unpublished	Marchant	Dabaso	39.2525	-3.5201	STR
Githumbi (2017; PhD)	Marchant	Kimana	37.6823	-2.5345	STR
unpublished	Marchant	Kitulu	34.656	-9.347	STR
unpublished	Marchant	Ksuasabuge	34.47	-1.174	STR
unpublished	Marchant	Luala	34.555	-9.294	STR
unpublished	Marchant	Marula	36.421	-0.194	STR
unpublished	Marchant	Mlanga	34.147	-9.457	STR

unpublished	Marchant	Ndanga	34.656	-9.347	STR
unpublished	Marchant	Rumuiku	37.3333	-0.1666	STR
unpublished	Marchant	Sangarwe	34.5757	-1.171	STR
unpublished	Marchant	Shidodo	34.025	-1.152	STR
Charman et al. (2013)	Phadtare	Dhakuri	79.9333	30.05	STR
Sanchez-Cabeza et al. (2014)	Sanchez-Cabeza	TEHUA-II	-94.49	15.6	STR
Swindles et al. (2018)	Swindles	Aucayacu	-74.39	-3.93	STR

Supplementary Table A2 Global database of recent rates of carbon accumulation (RERCA), cumulative peat mass (CM) and recent rate of carbon accumulation (RERCA) at 50, 100, and 150 years.

Site Code	*Bog/Fen Type*	*CM (g/cm^2) at 50 (yrs AD)*	*CM (g/cm^2) at 100 (yrs AD)*	*CM (g/cm^2) at 150 (yrs AD)*	*RERCA ($gC/m^2/yr$; CM50)*	*RERCA ($gC/m^2/yr$; CM100)*	*RERCA ($gC/m^2/yr$; CM150)*
Nadym	F	2.50	5.34	7.49	250.11	267.04	249.50
Shestakovo	F	2.57	3.99	4.66	257.22	199.69	155.29
Słowińskie Błota	B	1.00	1.40	1.57	100.11	69.88	52.36
Misten_Bog	B	0.66	1.17	1.70	66.48	58.40	56.71
Molhasul	B	2.04	5.19	8.34	204.36	259.51	277.90
Taul Muced	B	2.64	6.87	7.86	264.27	343.32	261.83
Bagno_Mikoleska	F	2.03	2.66	3.03	202.88	132.84	100.93
Pusczina_Mala	B	1.08	1.70	1.93	107.65	85.00	64.38
PK	B	0.74	1.01	1.20	73.98	50.48	39.96
Étang de la Gruyère 2f	B	1.75	2.39	2.75	175.49	119.73	91.64
Étang de la Gruyère 2k	B	1.21	2.29	2.73	120.53	114.37	91.10
Moor House	B	0.52	0.69	0.71	52.17	34.32	23.72
Mossdale	B	0.82	1.24	1.59	82.06	62.01	53.02
Nidderdale	B	0.69	1.24	1.48	69.45	62.11	49.48
Whitendale	B	1.26	1.88	2.32	126.31	94.17	77.22
BFA	B	0.85	1.61	2.24	84.74	80.59	74.54
BFB	B	1.01	1.51	1.92	100.99	75.36	63.95
Mannikjarvi	B	0.90	1.21	1.37	89.83	60.42	45.51
Stordalen_Kokfelt	F	0.55	0.88	1.04	55.33	44.13	34.69
Linje_Mire	F	1.85	3.08	3.63	185.27	154.12	121.13
ESTIBERE	B	1.16	1.66	2.04	115.83	82.83	68.02
Kolhütten	B	0.39	0.59	0.95	38.73	29.28	31.74
Pinet A	B	1.75	2.21	2.63	175.27	110.48	87.67
Pinet B	B	1.68	2.05	2.27	168.01	102.37	75.65
Pinet C	B	1.88	2.30	2.65	188.37	114.95	88.37
Honghe	F	3.36	5.60	6.20	336.11	279.75	206.75

Hongtu	F	1.52	2.36	2.63	152.10	118.19	87.61
Huyuan	F	1.93	4.09	4.42	193.44	204.73	147.33
Shenjiadian	F	6.52	8.79	9.76	652.34	439.31	325.28
Tuquiang	F	2.81	4.15	4.70	281.20	207.57	156.65
Hanhijanka	F	0.11	0.19	0.24	11.42	9.63	8.06
Luovuoma	F	0.85	2.15	3.51	84.83	107.62	116.99
Głęboczek	B	1.84	2.88	3.85	184.38	144.06	128.29
Linje	F	1.71	2.83	3.36	171.17	141.48	112.01
Balyduff	B	0.68	0.81	0.93	68.30	40.26	30.91
Connemara	B	1.00	1.64	2.49	99.78	81.80	83.12
Mull	B	0.61	0.98	1.16	61.43	49.14	38.57
Ocean Bog	B	0.84	1.46	2.00	83.58	73.16	66.82
Rybarenska slat	B	1.21	1.68	2.22	120.53	83.94	73.86
Thorne Moors	B	1.29	1.80	2.35	129.40	89.98	78.42
BM	B	0.61	0.88	1.25	61.47	43.94	41.72
EM	B	1.03	1.50	1.86	102.70	75.12	61.98
HW	B	0.36	0.54	0.67	35.72	26.88	22.44
RM	B	0.25	0.46	0.72	24.66	22.88	23.95
Degerö Stormyr	B	0.97	1.43	1.47	96.75	71.52	49.07
CHL-13	B	1.04	1.65	2.00	103.96	82.72	66.64
SM-1	B	0.82	1.22	1.56	82.39	61.14	51.94
SM-2	B	0.88	1.37	1.71	87.53	68.32	57.12
SM-3	B	1.15	1.95	2.24	115.50	97.69	74.77
Pedrido	B	1.28	2.01	2.26	128.47	100.41	75.42
Control, 6	B	0.86	1.33	1.52	86.10	66.50	50.83
Control, 7	B	1.46	1.66	1.78	145.60	83.01	59.42
Control, 8	B	1.10	1.64	1.79	110.46	82.00	59.59
SEMARNAT	B	0.57	0.90	1.11	56.73	45.02	37.00
Myranar 2	B	1.24	2.00	2.65	123.81	100.25	88.27
Craterpool_1	B	0.67	0.99	1.20	67.46	49.60	39.99
Craterpool_2	B	0.54	0.81	0.98	53.65	40.34	32.53

Dead_Island	B	0.72	1.08	1.42	72.08	53.97	47.44
Eagle_Bog	B/F	1.83	2.54	3.24	183.13	126.90	108.16
Electric_Bog	B	0.64	1.05	1.41	64.04	52.33	46.97
Instrument_Bog	B	0.33	0.58	0.92	32.83	28.76	30.81
Marooned	B/F	0.71	1.14	1.33	71.20	56.81	44.22
Nikka	B/F	0.53	0.84	1.10	52.56	41.80	36.60
Railway_Bog	B	0.68	1.21	1.84	67.76	60.39	61.33
Stordalen_Internal	F	0.40	0.77	1.11	39.54	38.61	37.13
Stordalen_Swindles	F	0.11	0.19	0.27	10.76	9.41	8.96
Malham_Tarn	B	1.23	1.68	2.13	122.89	84.00	71.04
Harjavalta	B	0.73	1.14	1.41	72.99	56.81	47.14
Hietajarvi	B	1.39	2.41	3.11	139.25	120.38	103.73
Outokumpu	B	1.06	1.68	2.08	106.33	84.08	69.42
Ind1	B	1.09	1.48	1.60	109.24	74.19	53.35
Ind2	B	0.64	1.01	1.32	63.51	50.51	44.04
Ind4	B	0.93	1.29	1.48	93.16	64.50	49.18
Ind5	B	0.46	0.77	1.03	45.56	38.46	34.18
Kev2	F	0.73	1.18	1.68	72.88	58.99	56.04
Kil	B	0.19	0.32	0.49	19.39	16.03	16.46
Kil2	F	0.29	0.48	0.69	29.33	23.76	22.95
LHL	B	0.68	1.19	1.27	68.46	59.32	42.26
LLH	B	1.20	1.76	2.07	120.17	87.83	69.16
LLL	B	0.61	1.02	1.41	61.00	51.14	47.03
SHL	B	1.23	1.49	1.74	123.47	74.58	58.12
SLH	B	1.23	1.75	1.98	123.11	87.47	65.86
SLL	B	1.00	1.25	1.36	99.84	62.38	45.40
Aéroport 1	F	0.49	1.06	1.52	48.55	52.92	50.79
Aéroport 4	F	0.47	1.04	1.50	46.58	51.76	50.09
Aéroport 5	F	0.98	1.56	1.91	98.30	78.11	63.52
Ours 1	F	0.53	0.78	1.03	53.01	38.81	34.44
Ours 4	F	0.42	0.89	1.42	41.98	44.33	47.42
Old Black Spruce 3	F	0.84	1.16	1.32	83.59	57.83	43.94

Sandhill Fen 4	F	0.42	0.76	0.92	42.31	38.03	30.77
DaS	B	1.91	2.82	3.73	190.78	141.04	124.46
DcC	B	0.63	0.99	1.35	63.43	49.74	44.99
HfC	B	1.25	2.37	3.50	125.16	118.54	116.58
HfS	B	2.38	3.45	4.53	237.68	172.49	150.85
Sidnaw	F	0.80	1.50	2.04	79.88	74.97	67.84
VC04-6	B	0.21	0.43	0.70	21.17	21.41	23.41
Petite_Bog	B	0.85	1.56	2.35	85.18	77.90	78.44
Burns_Bog	B	1.23	1.76	2.19	123.18	87.94	72.91
Surrey_Bog	B	1.56	2.18	2.59	156.40	108.97	86.36
ANZ	B	2.45	2.81	2.92	244.79	140.70	97.26
JPH	B	0.77	1.11	1.25	77.45	55.34	41.61
McK	B	2.07	2.59	2.94	207.11	129.50	98.04
McM	B	1.58	2.14	2.59	158.48	107.00	86.24
MIL	B	1.74	2.57	2.78	174.35	128.55	92.69
UTK*	B	2.29	3.14	3.99	229.29	156.83	133.16
AERO_1	F	0.73	1.11	1.34	72.92	55.48	44.65
BAIE_2_Garneau	B	0.77	1.15	1.38	77.50	57.34	45.94
Mer_Bleue_Garneau	B	1.66	2.03	2.23	165.74	101.43	74.40
Nordan	B	1.20	1.82	2.42	119.51	90.93	80.83
Fish_Creek	B	1.39	1.80	2.06	138.55	90.19	68.62
Point_lena	B	1.72	2.48	2.95	171.64	123.87	98.24
KUJU_PD2	B	1.33	1.90	2.47	133.33	95.00	82.22
Covey_Hill	B	3.26	5.18	6.42	325.60	259.22	214.04
Lac Le Caron RiP2	B	1.12	1.64	1.86	112.46	82.23	61.99
Mosaik RiP2	B	0.86	1.52	1.72	86.22	75.98	57.43
8T	B	1.88	2.26	2.32	187.80	112.99	77.42
K1P1	F	0.64	0.97	1.28	64.43	48.46	42.72
K1P2	F	0.72	1.04	1.28	72.03	52.05	42.65
K1P3	F	1.15	1.53	1.72	115.39	76.25	57.33
K2.1	F	1.00	1.36	1.63	100.17	67.97	54.31

K2.2	F	1.46	2.08	2.49	145.64	103.92	82.86
LG2.1	B	0.64	1.34	1.88	63.76	66.96	62.79
LG2.3	B	0.91	1.25	1.48	91.32	62.58	49.43
Rad1	B	1.14	1.92	2.34	113.72	95.91	78.14
Rad2	B	1.00	1.36	1.59	100.31	68.18	52.86
Rad3	B	0.61	1.09	1.66	61.47	54.33	55.33
BAIE_2_Sanderson	B	0.79	1.23	1.42	78.61	61.64	47.37
Lebel	B	1.17	2.21	2.85	116.68	110.26	95.04
Morts	B	0.71	1.15	1.50	71.36	57.34	50.00
Plaine	B	1.41	1.79	2.17	141.21	89.65	72.47
Red_Bay	B	0.88	1.36	1.71	87.81	67.90	56.99
Romaine	B	0.38	0.62	0.89	37.89	31.19	29.61
Vallee	B	0.59	1.00	1.32	59.24	50.20	43.97
Tasiusaq	F	0.46	0.71	0.92	46.22	35.42	30.78
Coastal Fen A	F	0.93	2.34	3.76	92.88	117.22	125.34
Coastal Fen B	F	0.53	0.80	0.92	53.33	39.90	30.75
TFS1	F	0.66	0.95	1.08	65.90	47.57	35.86
TFS2	F	0.46	1.11	1.51	46.24	55.36	50.43
Anzac 1	B	1.08	1.93	2.56	107.61	96.57	85.31
Anzac 2	B	1.25	1.82	2.17	125.28	91.01	72.47
Moose Lake	B	1.10	1.61	1.99	110.14	80.46	66.24
Patuanak	B	1.43	1.94	2.47	142.63	96.96	82.17
Edson	F	1.35	1.65	1.95	135.43	82.66	64.98
Hondo	F	0.78	1.31	1.41	78.34	65.57	47.15
Saulteaux	F	0.83	1.21	1.58	83.01	60.74	52.54
Big Run	F	2.11	3.09	3.74	211.44	154.29	124.60
Cranesville	F	1.85	2.27	2.54	184.94	113.53	84.61
Marcell	B	1.26	1.76	2.00	126.06	87.95	66.52
Tamarack	F	1.15	1.57	1.81	115.07	78.42	60.49
Tub Run	F	1.67	2.33	2.55	167.22	116.34	85.14
BP	B	0.80	1.07	1.20	80.45	53.52	39.86
MP	B	0.75	1.42	1.86	75.04	70.94	62.09

CA	B	0.52	0.94	1.37	51.55	47.05	45.55
CH	B	0.88	1.18	1.48	87.57	58.97	49.43
PL	B	0.79	1.29	1.80	78.57	64.54	59.86
SD	B	0.50	1.01	1.52	50.39	50.69	50.80
TG	B	0.79	1.29	1.80	78.58	64.54	59.86
Karukinka_A_B	B	0.57	0.78	0.99	57.48	39.01	32.91
Pulpito	B	0.49	0.85	1.03	49.38	42.44	34.22
Tierra_Australis	B	0.74	0.93	1.05	74.11	46.59	35.12
Sebangau_1A	B	0.87	1.06	1.21	86.51	53.19	40.28
Sebangau_1B	B	0.31	0.38	0.46	31.22	19.22	15.22
Sebangau_2A	B	0.58	0.90	1.24	58.27	45.25	41.18
Sebangau_2B	B	1.78	2.36	2.94	177.56	118.08	97.95
Sebangau_3A	B	0.88	1.21	1.44	88.14	60.45	48.12
Sebangau_3B	B	0.80	1.26	1.72	80.21	63.01	57.28
Sebangau_4A	B	1.64	2.37	3.28	164.17	118.53	109.28
Sebangau_5A	B	2.62	3.38	4.36	262.04	169.22	145.47
Sebangau_5B	B	1.22	1.57	1.78	122.41	78.36	59.35
Amsterdam Island	B	0.59	0.91	1.34	59.19	45.41	44.57
INP	B	4.79	8.96	13.14	478.60	448.03	437.84
SONP	B	5.15	9.43	13.71	515.00	471.40	456.86
Dabaso	Peat Swamp	6.65	7.39	7.89	664.61	369.46	263.04
Kimana	B	6.09	7.12	7.55	608.92	355.84	251.74
Kitulu	B	2.73	4.09	5.46	272.86	204.62	181.88
Ksuasabuge	Peat Swamp	3.03	4.09	5.15	303.23	204.63	171.65
Luala	B	2.51	3.04	3.55	251.48	152.07	118.36
Marula	Peat Swamp	4.20	6.49	7.08	419.62	324.71	236.14
Mlanga	B	3.67	5.18	6.70	366.65	259.23	223.42
Ndanga	Peat Swamp	2.20	2.72	3.20	219.74	136.19	106.68
Rumuiku	Peat Swamp	5.24	6.01	6.72	524.32	300.32	224.01
Sangarwe	B	6.53	14.70	22.87	652.76	734.87	762.24
Shidodo	B	10.19	11.37	12.55	1019.34	568.71	418.49
Dhakuri	F	0.60	1.12	1.50	60.16	55.89	50.08

TEHUA-II	B	0.69	1.46	2.03	69.37	72.83	67.52
Aucayacu	B	1.41	2.36	2.54	140.70	118.13	84.65

Supplementary Table A3. Identified volcanic ash layers (tephra) from previous studies, applied to cores from this study.

Previous Studies	*AI*	*MBII*	*Hb*	*HI*	*MBI*	*Ha*	*RI*
Stern, 2008	3369 - 2863 (3116)	5289 - 3234 (4261.5)	6544 - 5790 (6167)	7960 - 7423 (7691.5)	10641 - 8183 (9412)	10550 - 10268 (10409)	15776 - 14041 (14908.5)
Kilian et al., 2003	3879 - 3596	4254	-	7795 - 7707	9175 - 9009	-	> 15384
Mansilla et al., 2016	-	4440 - 3800 (4150)	6544 - 5790 (6130)	7990 (8135 - 7870)	10200 - 9690 (9910)	10760 - 10260 (10530)	15215 - 14670 (14980)

This Study	*AI*	*MBII*	*Hb*	*HI*	*MBI*	*Ha*	*RI*
BP	-	4504 (189)	6443 (261)	8342 (371)	8920 (419)	10003 (503)	14903 (737)
PAN	2654 (57)	3232 (71)	6587 (179)	7963 (265)	8508 (297)	11068 (491)	-
MP	2540 (79)	5007 (125)	5897 (141) & 6673 (163)	7164 (181)	8926 (247)	-	-
JB	2926 (293)	4427 (439)	-	-	-	-	-
SJ	-	-	-	-	-	-	-
CP2	-	-	-	8073 (291)	8073 (291)	-	-
CP	N/A (44)	N/A (167)	N/A (213)	N/A (231)	-	-	-
FP	N/A (89)	-	-	N/A (299)	N/A (299)	-	-
RP	-	N/A (135)	N/A (203)	-	-	-	-